Tectonics

RESEARCH ARTICLE
10.1029/2022TC007706

Paleomagnetic Rotations in the Northeastern Caribbean Region Reveal Major Intraplate Deformation Since the Eocene

Leny Montheil[1], Mélody Philippon[2], Philippe Münch[1], Pierre Camps[1], Bram Vaes[3], Jean-Jacques Cornée[2], Thierry Poidras[1], and Douwe J. J. van Hinsbergen[3]

[1]Geosciences Montpellier (UMR 5243, CNRS/UM/Université des Antilles), Université de Montpellier, Montpellier, France, [2]Geosciences Montpellier (UMR 5243, CNRS/UM/Université des Antilles), Université des Antilles, Pointe-à-Pitre, France, [3]Department of Earth Sciences, Utrecht University, Utrecht, The Netherlands

Key Points:

- Since the late Eocene the Puerto Rico-Northern Lesser Antilles block underwent ≃45° of counterclockwise rotation
- During the Miocene the opening of the Anegada Passage split this block in two and accommodated part of their differential rotation rate
- Our results imply intraplate motion of a forearc sliver over 500 km with profound effects on Paleogene Caribbean paleogeography

Supporting Information:

Supporting Information may be found in the online version of this article.

Correspondence to:

L. Montheil,
leny.montheil92@gmail.com

Citation:

Montheil, L., Philippon, M., Münch, P., Camps, P., Vaes, B., Cornée, J.-J., et al. (2023). Paleomagnetic rotations in the northeastern Caribbean region reveal major intraplate deformation since the Eocene. *Tectonics*, *42*, e2022TC007706. https://doi.org/10.1029/2022TC007706

Received 7 DEC 2022
Accepted 19 JUN 2023

Author Contributions:

Conceptualization: Leny Montheil, Mélody Philippon, Jean-Jacques Cornée, Douwe J. J. van Hinsbergen
Data curation: Leny Montheil, Mélody Philippon, Pierre Camps, Douwe J. J. van Hinsbergen
Formal analysis: Leny Montheil, Mélody Philippon, Pierre Camps, Bram Vaes, Thierry Poidras, Douwe J. J. van Hinsbergen
Funding acquisition: Mélody Philippon, Philippe Münch, Jean-Jacques Cornée

Abstract Relative Caribbean-North American plate motion is partitioned over the trench and intra-Caribbean plate faults that bound large scale tectonic blocks. Quantifying the kinematic evolution of this tectonic corridor is challenging because much of the region is submarine. We present an extensive regional paleomagnetic data set (1,330 cores from 136 sampling locations) from Eocene and younger rocks of the northern Lesser Antilles, the Virgin Islands, and Puerto Rico, and use a statistical bootstrapping approach to quantify vertical axis block rotations. Our results show that the Puerto Rico–Virgin Island (PRVI) block and the Northern Lesser Antilles (NoLA) block formed two coherently rotating domains that both underwent at least 45° counterclockwise rotation since the Eocene. The first ~20° occurred in tandem in late Eocene and Oligocene time, after which the blocks were separated in the Miocene by the opening of the Anegada Passage. The last 25° of rotation of the PRVI block ended in the middle Miocene, whereas the NoLA block rotated slower, until the latest Miocene. The boundary between the NoLA block and a non-rotated Southern Lesser Antilles was likely the Monserrat-Harvers fault zone. These results require hundreds of kilometers of intra-Caribbean motions with oroclinal bending of the trench or forearc sliver motion along the curved plate boundary as endmembers. These data invite a critical re-evaluation of the kinematic reconstruction of Caribbean-North American plate motion. The consequent changes in paleogeography may provide a new view on the enigmatic eastern Caribbean paleo-biogeography and the Paleogene dispersal of South American mammals toward the Greater Antilles.

1. Introduction

Motion between the North American and Caribbean plates is distributed in the northeastern part of the intervening plate boundary over a series of major faults that surround and dissect ancient and active volcanic arc complexes built on the oceanic Caribbean plate lithosphere (Figure 1) (e.g., Byrne et al., 1985; Román et al., 2021; Wessels, 2019). This intraplate deformation occurs in a region where the plate boundary curves, from nearly orthogonal subduction at the Lesser Antilles trench to pure strike-slip motion northwest of Puerto Rico (Calais et al., 2023; DeMets et al., 2000) (Figure 1). The present-day kinematics of the northeastern Caribbean tectonic corridor, which consists of connected strike-slip faults with transpressional and transtensional step-overs are reasonably well-constrained by seismicity (van Rijsingen et al., 2021) and GPS (Mann et al., 2002; Symithe et al., 2015) data, respectively. However, questions such as when and how this distributed plate boundary developed and evolved, and how much displacement has been accommodated by intraplate deformation remain debated because most of the crustal deformation archives are submarine, even though extensive efforts have been made with offshore studies in the Greater and Lesser Antilles (Boucard et al., 2021; Garrocq et al., 2021; Granja Bruña et al., 2010; Grindlay et al., 2005; Laurencin et al., 2017, 2019; ten Brink et al., 2009).

Quantifying the kinematic evolution of Caribbean intraplate deformation is key for understanding the dynamics of strain partitioning in oblique subduction zones (e.g., Philippon & Corti, 2016) and for the reconstruction of Caribbean-North American plate motion (Boschman et al., 2014). This kinematic restoration is of particular interest to reconstruct the enigmatic paleogeographic evolution of the eastern Caribbean region. Despite being an oceanic plate, a late Paleogene "GAARLandia" landbridge has been hypothesized between the Greater Antilles islands and South America to explain dispersal patterns of terrestrial fauna mainly based on paleontological evidence and on the proposal of a major emersion phase of the Aves Ridge at 35-33 Ma (Iturralde-Vinent & MacPhee, 1999). Recently, onshore and offshore geological and geophysical data have shown that intraplate

Investigation: Leny Montheil, Mélody Philippon, Philippe Münch, Jean-Jacques Cornée, Douwe J. J. van Hinsbergen
Methodology: Leny Montheil, Mélody Philippon, Pierre Camps, Bram Vaes, Jean-Jacques Cornée, Thierry Poidras, Douwe J. J. van Hinsbergen
Project Administration: Philippe Münch
Resources: Leny Montheil, Mélody Philippon, Thierry Poidras, Douwe J. J. van Hinsbergen
Software: Leny Montheil, Pierre Camps, Bram Vaes, Thierry Poidras, Douwe J. J. van Hinsbergen
Supervision: Mélody Philippon, Philippe Münch, Pierre Camps, Jean-Jacques Cornée, Thierry Poidras, Douwe J. J. van Hinsbergen
Validation: Leny Montheil, Mélody Philippon, Pierre Camps, Bram Vaes, Thierry Poidras, Douwe J. J. van Hinsbergen
Visualization: Leny Montheil, Mélody Philippon, Douwe J. J. van Hinsbergen
Writing – original draft: Leny Montheil, Mélody Philippon, Jean-Jacques Cornée, Douwe J. J. van Hinsbergen
Writing – review & editing: Leny Montheil, Mélody Philippon, Philippe Münch, Pierre Camps, Bram Vaes, Jean-Jacques Cornée, Douwe J. J. van Hinsbergen

deformation may have formed and destroyed emerged areas further to the east, in the Lesser Antilles, and that this region may have contributed to the formation of paleo-islands (Boucard et al., 2021; Cornée et al., 2021; Legendre et al., 2018; Philippon, Cornée, et al., 2020). In this paper, we report an extensive regional paleomagnetic data set that we collected from Puerto Rico to Martinique to aid kinematic restoration, and to determine the timing of deformation through vertical axis rotation analysis of Paleogene and younger sedimentary and igneous geological records.

In the Greater Antilles, large counterclockwise rotations have been recognized since the 80s (Mann & Burke, 1984) and two concept have been proposed to account for such rotation with (a) rotation of a large Greater Antilles block around a pivot located at the Bahamas Bank collision point (Wallace et al., 2009) and (b) rotation of smaller sized fault bounded blocks (MacDonald, 1980). In the eastern Greater Antilles and in the Lesser Antilles, previous studies found that rotations affected islands of as much as 45° counterclockwise rotation since the Eocene in Puerto Rico (Reid et al., 1991; van Fossen et al., 1989) and as much as 15°–25° counterclockwise rotation since the Oligocene in St. Barthélemy (Philippon, van Hinsbergen, et al., 2020). To the contrary, the southern island of Mayreau in the Grenadines does not show evidence of rotation since the middle Eocene (Speed et al., 1997). In this study, we integrate these isolated data sets into an extensive paleomagnetic survey, carried out in the northeastern Caribbean region. We estimate rotations around a vertical axis from rocks exposed on islands within the zone of trench curvature, that are part of the active deformation belt (Puerto Rico, British Virgin Islands), as well as from zones surrounded by faults that are not known to be active (St Martin, Anguilla, Antigua, Martinique). We use these rotations to quantify the evolution of upper-plate internal deformation of the northeastern Caribbean plate and test the tectonic scenarios proposed by earlier studies. Moreover, we address a recently unearthed problem in classical paleomagnetic approaches, outlying that the statistical differences between datasets might not always bear tectonic meaning (Rowley, 2019). In these approaches, the grand' mean paleomagnetic direction of a given data set is compared with a reference direction or pole predicted by a (global) apparent polar wander path (APWP) (e.g., Torsvik et al., 2012). Nevertheless, more than half of the paleomagnetic poles of the global APWP by Torsvik et al. (2012) are statistically different from the APWP itself due to the use of paleomagnetic data sets of unequal size (Rowley, 2019). To overcome this problem, we apply here for the first time a statistical bootstrapping approach developed by Vaes et al. (2022) in which the studied paleomagnetic data set is compared to a reference pole that is defined by the same number of Virtual Geomagnetic Poles (VGP) included in the studied data set.

2. Geological Setting

The Caribbean plate consists of an oceanic lithosphere intruded and overlain by a large igneous province and magmatic arcs, surrounded by the North and South American plates and continents (Bouysse et al., 2020; Romito & Mann, 2021; Steel & Davinson, 2021). To the east, the Caribbean plate is bounded by the Lesser Antilles subduction zone (Figure 1). This subduction accommodates nearly E-W convergence between the North and South American plates and the Caribbean plate and was initiated during an Eocene change in the relative motion between the Caribbean Plate and the Americas from NE to E (Boschman et al., 2014; Pindell & Dewey, 1982). To the north, the Lesser Antilles trench curves and connects to the Puerto Rico trench, where highly oblique subduction occurs with an angle of up to 77° (Calais et al., 2023; DeMets et al., 2000; Symithe et al., 2015) (Figure 1). Further west, to the north of Hispaniola, the subduction trench connects to a strike-slip-dominated plate boundary around the southern tip of the Bahamas bank (Figure 1). This bank consists of a North American and thinned continental crust and perhaps volcanically thickened oceanic crust overlain by a thick (5–10 km), Jurassic to Neogene, carbonate platform (Carew et al., 1997; Iturralde-Vinent, 1994; Rodriguez-Zurrunero et al., 2019). This SE trending bathymetric feature progressively accreted on the Great Arc of the Caribbean (GAC, Burke, 1988) since the Eocene, potentially triggering counterclockwise rotation of the Greater Antilles (Mann et al., 2005).

The Septentrional-Oriente strike-slip fault zone (SOFZ, Figure 1) marks the separation between the Caribbean plate and the Cuban segment, which accreted to the North American plate since the late Eocene following the accretion of the Bahamas Bank (Iturralde-Vinent et al., 2008). The SOFZ bounds the Cayman Trough, a pull-apart basin that opened since 49 Ma (Leroy et al., 1996, 2000). Magnetic anomalies from the oceanic crust within the Cayman Trough show that the modern North America-Caribbean plate motion rate of ~2 cm per year has pertained since the Eocene (Leroy et al., 2000). The southern Cayman Trough is marked by two active strike-slip faults, the Swan fault to the west and the Walton fault to the east. This latter connects to the active Enriquillo

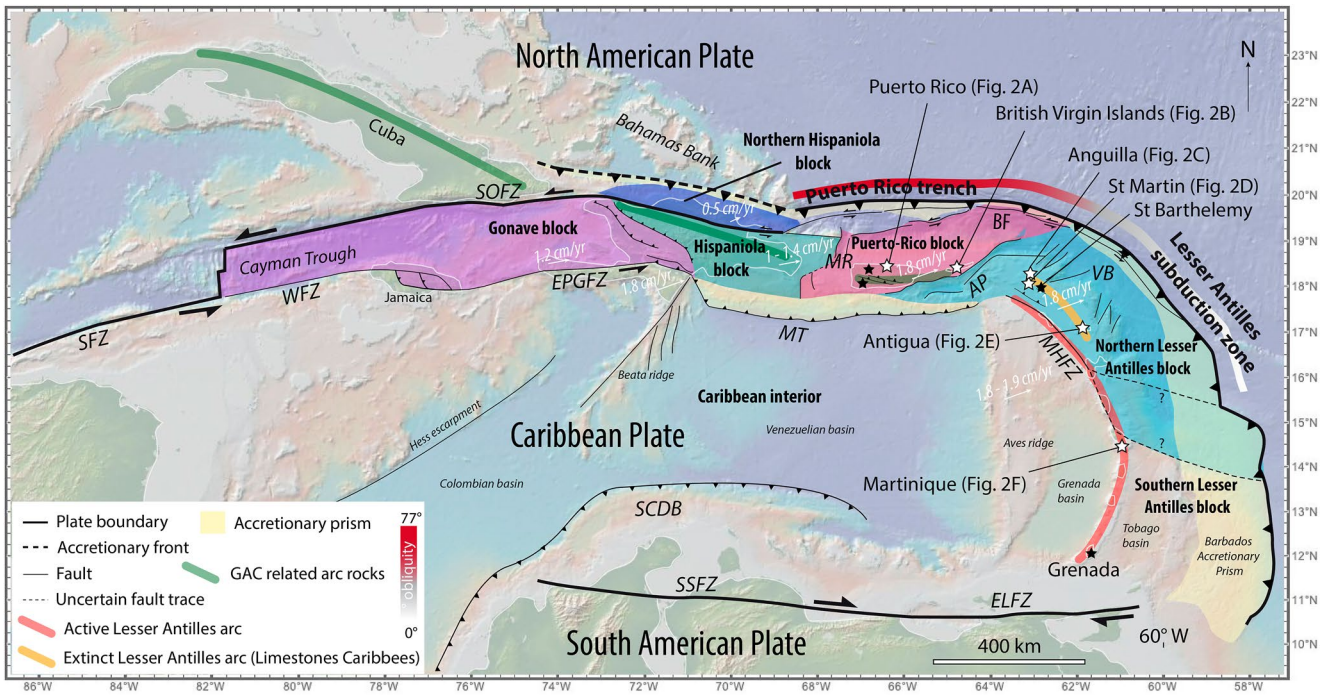

Figure 1. Structural map of the Caribbean plate with the potential tectonic blocks of the north-eastern Caribbean based on geodesy and marine geophysical records (Symithe et al., 2015). White arrow: GPS velocities of the north-eastern Caribbean blocks relative to North America (from Calais et al. (2016) and Symithe et al. (2015)). The question mark outlines the probable but undefined southern limit of the Northern Lesser Antilles block. AP: Anegada passage; BF: Bunce Fault; ELPZ: El Pilar Faut Zone; EPGFZ: Enriquillo Plantain Fault Zone; MHFZ: Montserrat-Harvers Fault Zone; MT: Muertos Trough; MR:Mona Rift; SCDB: Southern Caribbean Deformed Belt; SFZ: Swan Fault Zone; SOFZ: Septentrional Oriente Fault Zone; SSFZ: San Sebastian Fault Zone; VB: V-shaped basins; WFZ: Walton Fault Zone.

Plantain Garden strike-slip fault zone (EPGFZ), that bounds the Gonave microplate (Benford, DeMets, & Calais, 2012; Calais et al., 2016; Leroy et al., 2015) through a series of restraining bends in Jamaica (Mann, 2007) (Figure 1). The activity of both the Walton fault and EPGFZ shows that not all the Caribbean-North American plate motion steps over at the mid-Cayman spreading center (Corbeau et al., 2016; Leroy et al., 2000; Oliviera de Sa et al., 2021). Southeast of Hispaniola, the EPGFZ connects to the Muertos Trough, an E-W trending, north dipping thrust fault (Byrne et al., 1985; Granja-Bruna et al., 2014). Between Hispaniola and Puerto Rico lies an active extensional basin known as the Mona rift (Mondziel et al., 2010). Farther east, the Muertos Trough connects to the NE-SW trending Anegada Passage with a presumed transtensional motion component (Laurencin et al., 2017). To the northeast, the Anegada Passage connects to the trench-parallel Bunce fault, a sinistral strike-slip fault located between the accretionary prism and a rigid backstop that separates a narrow forearc sliver from the Caribbean plate (Laurencin et al., 2019) (Figure 1). To the southeast, the Monserrat-Harvers fault zone (MHFZ) connects from the Anegada passage and the Muertos trough. This fault is an en-echelon fault system on which normal activity has been recognized and that is thought to run parallel to the active Lesser Antilles arc (Calcagno et al., 2012; Feuillet et al., 2010, 2011). The southeastern prolongation of this fault, toward the subduction trench, is still debated. Some authors postulate that the MHFZ is relayed by the normal faults of the Marie-Galante basin (Cornée et al., 2023; Feuillet et al., 2010) while other postulate that the fault extends through Dominica and Martinique and north of the Barbados ridge (Gomez et al., 2018) (Figure 1). Lopez et al. (2006) postulated that the MHFZ is still accommodating strike-slip displacement of a fore-arc sliver, but more recent geodetic data show no active relative motion across the fault (Symithe et al., 2015).

These large faults surround crustal blocks that are not entirely rigid, as there is evidence for smaller-scale deformation within the blocks (Boucard et al., 2021; Cornée et al., 2021; Legendre et al., 2018; Mann et al., 2005; Noury et al., 2021; ten Brink et al., 2020). Nonetheless, in the absence of evidence for major intra-block deformation, we will start our analysis with the assumption that the blocks outlined in Figure 1 are coherently rotating tectonic blocks, unless our paleomagnetic data demonstrate otherwise. These blocks include, from east to west: the Southern Lesser Antilles (SoLA) block, the Northern Lesser Antilles (NoLA) block, the Puerto Rico-Virgin Islands

(PRVI) block, the Hispaniola block, the Northern Hispaniola block and the Gonave block (Figure 1). These blocks bound the rigid Caribbean plate interior, that is composed of a Mesozoic oceanic seafloor, found in Colombian and Venezuelan basins, that is overlaid by the Cretaceous Caribbean Large Igneous Province, recognized in the Nicaraguan rise, the Beata ridge, and the Aves ridge (Kerr et al., 1997; Mauffret & Leroy, 1997, 1999; Pindell & Kennan, 2009; Romito & Mann, 2021; Schwindorfska et al., 2016). East of the Aves ridge, the Grenada basin opened and accommodated oceanic spreading in its southern part from ~48 to 38 Ma (Garrocq et al., 2021). This basin is separated from the Tobago basin by the active southern Lesser Antilles arc (Aitken et al., 2011; Allen et al., 2019). The Grenada basin is considered either as a back-arc basin of the ancient Lesser Antilles Arc (Allen et al., 2019; Garrocq et al., 2021; Padron et al., 2021) or as a forearc basin of the GAC (Aitken et al., 2011). These basins and volcanic islands form the Southern Lesser Antilles block. No major structure is observed between this block and the Caribbean interior indicating that they should be considered as part of the same coherent block.

At present-day, GPS measurements do not demonstrate relative motion between the Puerto Rico-Virgin Islands, the Northern Lesser Antilles blocks, and the Caribbean interior (Symithe et al., 2015; Figure 1). A differential motion ranging from 0.5 to 1.5 cm per year is recognized between these coherent blocks and the Hispaniola, Northern Hispaniola and Gonave blocks (Benford, Tikoff, & DeMets, 2012; Symithe et al., 2015; Figure 1). The differential motion is accommodated by the E-W extending Mona rift, that opened following the indentation of the Bahamas bank into the Hispaniolan blocks (Chaytor & Ten Brink, 2010), and by sinistral strike slip on the EPGFZ (Mann et al., 2005).

The Puerto Rico-Virgin Islands and Northern Lesser Antilles blocks display evidence of internal deformation. Unconformities recognized in the stratigraphic records of islands and the offshore basins attest to this: in Puerto Rico, a sedimentary hiatus and an angular unconformity are observed between an Oligocene to Pliocene arched sedimentary sequence (Grindlay et al., 2005) and a Cretaceous to middle Eocene basement, composed of GAC-related deformed rocks (Figure 1). This basement is structured by the Southern and Northern Puerto Rico Fault Zone, whose activities since the Oligocene are still debated (Laó-Dávila, 2014). Within the Northern Lesser Antilles block mid-Eocene thrusting has been documented (Philippon, Cornée, et al., 2020), followed by strong subdsidence and uplift in the Oligocene and Miocene, respectively (Cornée et al., 2021). The British Virgin Islands underwent a more dramatic tectonic history which involved an Eocene to Oligocene exhumation of undeformed Paleogene plutons that intrude a highly deformed, amphibolite to greenschist-facies Cretaceous arc sequence (Román et al., 2021; Schrecengost et al., 2009; Wilson et al., 2019).

The islands that we targeted for paleomagnetic sampling (i.e., Puerto Rico, British Virgin Islands, Anguilla, Saint-Martin, Antigua, and Martinique) expose plutonic, volcanic, and (volcano-)sedimentary rocks that formed arc volcanoes and that are overlain by limestone sequences post-dating these volcanoes (e.g., Hu et al., 2022; Lidiak & Anderson, 2015; Montheil et al., 2023). The Lesser Antilles Arc is divided in two branches: the northeastern and extinct Eocene-Oligocene branch that is recognized in the "Limestone Caribbees" islands (i.e., Antigua, St Barthélemy, Saint-Martin and Anguilla) and the western late Oligocene to present-day active branch that is recognized on the island of Saba, Saint-Kitts and Nevis, Monserrat, Guadeloupe, Dominica, Martinique, Saint-Lucia, the Grenadines and Grenada (e.g., Allen et al., 2019; MacDonald et al., 2000; Montheil et al., 2023; Nagle et al., 1976) (Figure 1). Eocene to Miocene arc-related rocks are well exposed on the British Virgin Islands (Wilson et al., 2019), Saint-Martin (Noury et al., 2021), Antigua (Montheil et al., 2023) and in Martinique (Germa et al., 2011) (Figures 2 and 3). These arc-related rocks are overlain by Oligocene to Pliocene marine limestones with minor detrital units on Puerto Rico (Renken et al., 2002), Anguilla, Saint-Martin (Cornée et al., 2021), and Antigua (Montheil et al., 2023) (Figures 2 and 3). In Martinique, magmatism lasted from the late Oligocene to the present day and three episodes have been distinguished (late Oligocene-early Miocene, middle to late Miocene, Pliocene to Present; Germa et al., 2011) (Figures 2 and 3).

3. Paleomagnetic Sampling

For paleomagnetic analysis, we targeted undeformed, mid-Eocene to late Miocene plutonic, volcanic, and sedimentary rocks. A total of 1,330 samples, distributed over 136 sampling locations, were collected (Figure 3 and Table 1). Standard core samples were collected with a gasoline-powered portable drill and oriented in situ with a magnetic and a sun compass for sedimentary and magmatic rocks, respectively. 50 samples were drilled in the laboratory from oriented block samples. The orientation of all magnetic compass measurements has been corrected for the regional magnetic declination varying between 13.0° and 15.2° depending on the island and year

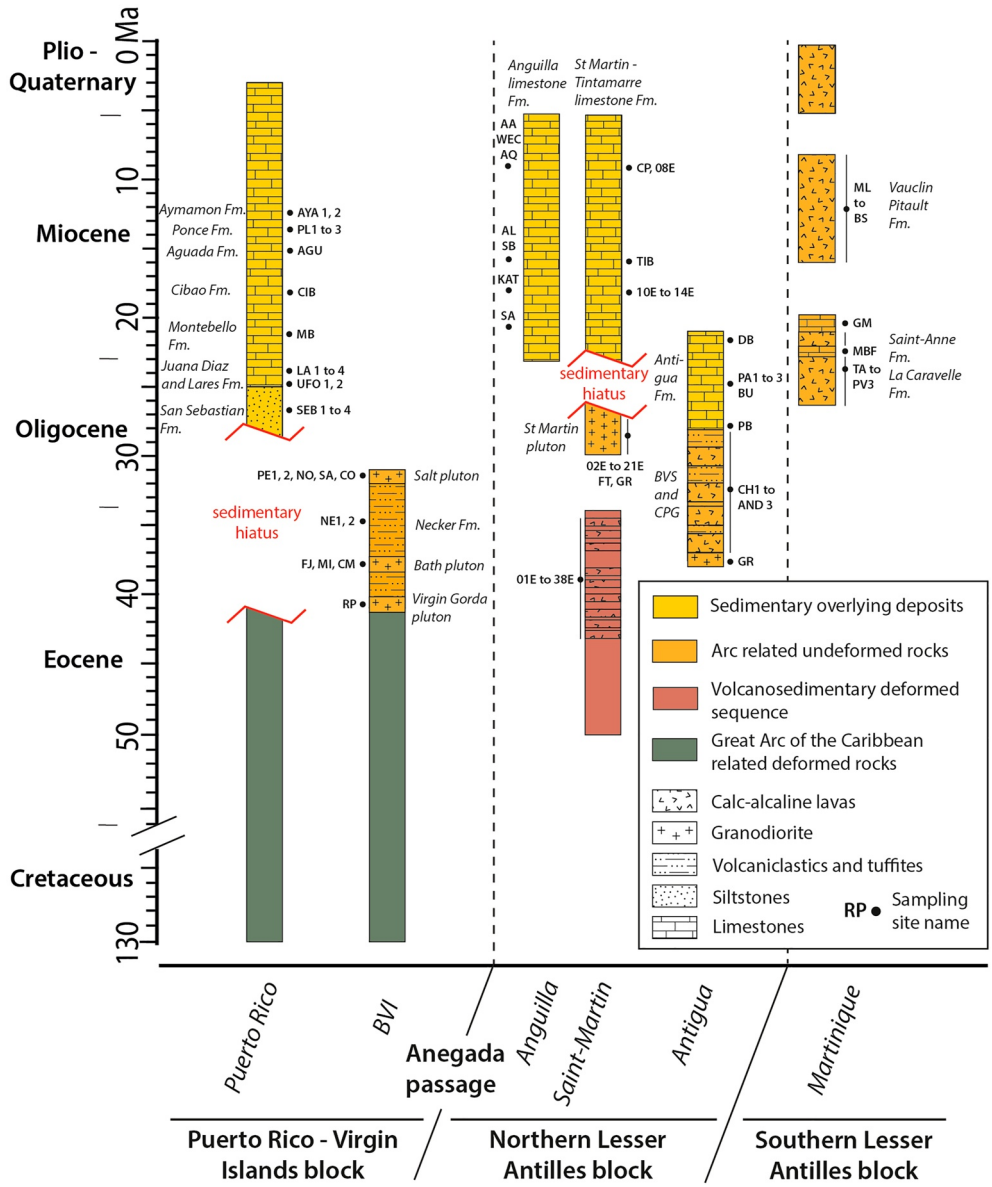

Figure 2. Schematic stratigraphy of the geological units exposed in Puerto Rico (from Laó-Dávila (2014) and Wilson et al. (2019)), British Virgin Islands (BVI, from Wilson et al. (2019)), Anguilla, Saint-Martin (from Cornée et al. (2020) and Noury et al. (2021)), Antigua (BVS: Basal Volcanic Suite, CPG: Central Plain Group, from Montheil et al. (2023)) and in Martinique (from Germa et al. (2011)).

of sampling. The tectonic tilt has been corrected according to the exposure dip of initially sub horizontally deposited strata for sedimentary units (Table 1). We corrected the magmatic units of Antigua by means of the mean strata dip of the synchronously deposited sedimentary unit (Central Plain Group, 10°NE, Montheil et al., 2023). In Saint-Martin, we corrected the Oligocene granodiorite specimens following the mean bedding of the Eocene sedimentary units that are intruded by the plutons, as these Eocene and Oligocene units are supposed to be tilted similarly during the late Oligocene (40°SE, Noury et al., 2021) (Table 1 and Figure 3). We checked this tectonic tilt with inclination consistency. To optimize the chance that we collected as many independent readings of the geomagnetic field as possible and optimally represent and averaged paleosecular variation, we collected one sample per bed in carbonate and silt units, and one sample every 3–10 m in granodiorites following recommendations in Gerritsen et al. (2022) (Figure 4). Moreover, in granodiorites, we focused as much as possible on collecting samples from mafic enclaves that were finer grained and richer in magnetic minerals. Large sequences of individual lavas were generally not available, and only a limited number of magnetic spot readings have been

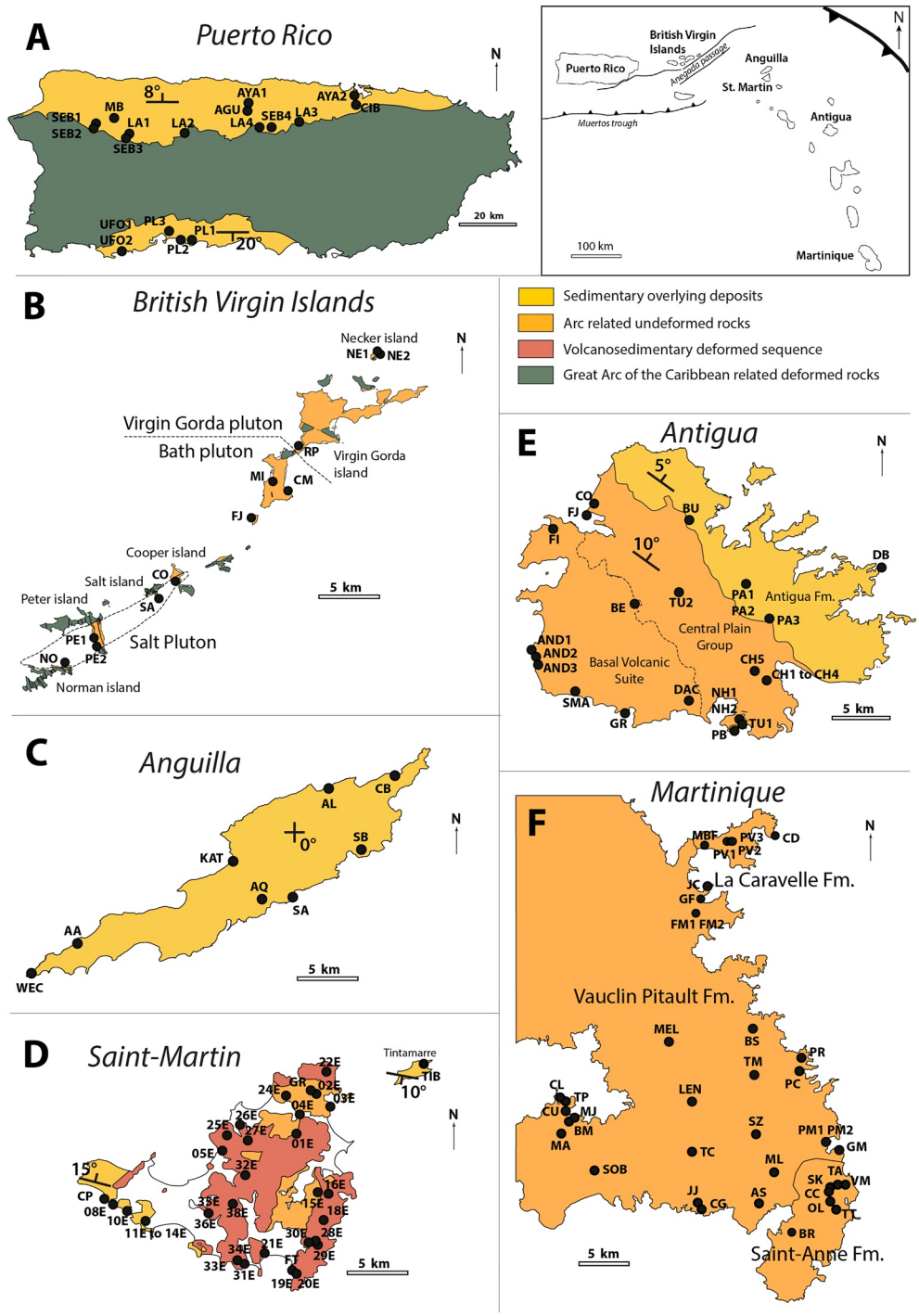

Figure 3. Simplified geological map of the targeted islands and location of the sampling locations. (a) Puerto Rico modified from Laó-Dávila (2014) and Wilson et al. (2019); (b) British Virgin islands modified from Wilson et al. (2019); (c) Anguilla, modified from Cornée et al. (2020), (d) Saint-Martin, modified from Noury et al. (2021), (e) Antigua, modified from Montheil et al. (2023), and (f) Martinique, modified from Germa et al. (2011).

collected. We collected 5 to 7 samples per lava, dyke, or sill to test the reproducibility of the magnetic reading as expected for rapidly cooled magmatic units (Figure 4).

In Puerto Rico, we sampled upper Oligocene to upper Miocene sediments that comprise non-marine silts at the base grading to reef and platform limestones and marine mudstones at the top (Ortega-Ariza et al., 2015;

Tectonics
10.1029/2022TC007706

Table 1
Sampling Location Mean Direction and Statistical Parameter per Sampling Location and per Collection Mean

Sampling location							Geographic				Tectonic								
Puerto Rico	Lithology	Age	Lat.	Long.	Ni	Pol.	D	ΔD_x	I	ΔI_x	D	ΔD_x	I	ΔI_x	K	A95	$A95_{min}$	$A95_{max}$	Bedding
87R047	Limestone	Pliocene	See Reid et al. (1991)		5	R	180.4	20.1	−22.7	34.9	Not corrected				16.2	19.6	6.3	29.8	
87R046					6	R	171.2	26.7	−9.4	52.2					7.3	26.6	5.9	26.5	
87R045					6	R	185.6	25.0	−44.2	28.4					9.9	22.4	5.9	26.5	
87R044					5	R	177.7	20.8	−34.0	30.1					16.1	19.7	6.3	29.8	
			Collection mean direction		22		358.3	11.9	28.0	19.2					8.2	11.2	**3.5**	**11.7**	
PL1	Limestone	Langhian to Messinian [2] [3]	17.9853	−66.67	6	R	181.1	11.5	−28.3	18.4	181.1	12.1	−33.3	17.8	34.9	11.5	5.9	26.5	90/20
PL2			17.9794	−66.702	1	R	193.4		−23.4		194.0		−28.2						
PL3			17.9875	−66.827	7	N	11.1	13.6	47.5	14.1	12.4	15.2	52.4	13.4	23.7	12.7	5.5	24.1	270/8
87R040		Serravalian [1] [3]	See Reid et al. (1991)		5	R	157.1	8.0	−2.8	16.0	Not corrected				92.3	8.0	6.3	29.8	
87R037					3	N	337.8	19.8	18.7	36.0					41.0	19.5	7.7	41.0	
AYA 1			18.4267	−66.475			No meaningful results												
AYA 2			18.4447	−66.144	11	R	187.5	7.2	−18.2	13.2	187.3	6.9	−14.2	13.1	50.3	6.9	4.8	19.2	270/8
AGU		Langhian [1] [3]	18.4122	−66.49			No meaningful results. outlier												
			Collection mean direction		32		359.9	12.2	29.4	19.2	359.9	12.5	30.7	19.3	5.5	12.0	**3.0**	**9.2**	
87R026		Burdigalian [1] [3]	See Reid et al. (1991)		4	N	335.9	25.8	46.3	27.6	Not corrected				17.4	22.7	6.9	34.2	
CIB			18.3947	−66.226	13	N	355.3	24.8	38.0	32.9	355.5	24.2	34.0	35.0	4.6	22.9	4.4	17.1	270/8
87R024–34		Aquitanian [1] [3]	See Reid et al. (1991)		5	R, N*	326.3	14.4	30.1	22.5	Not corrected				31.5	13.9	6.3	29.8	
87R021					3	N	338.1	21.0	19.2	37.9					36.7	20.6	7.7	41.0	
MB			18.3322	−66.946			No meaningful results. outlier												270/8
			Collection mean direction		24		343.8	8.1	33.5	11.8	344.2	8.0	31.5	12.1	16.1	7.6	**3.4**	**11.1**	

10.1029/2022TC007706

Table 1
Continued

Sampling location							Geographic				Tectonic								
Puerto Rico	Lithology	Age	Lat.	Long.	Ni	Pol.	D	ΔD_x	I	ΔI_x	D	ΔD_x	I	ΔI_x	K	A95	$A95_{min}$	$A95_{max}$	Bedding
	Limestone	Upper Chattian [1] [3]	See Reid et al. (1991)		5	N	347.4	19.6	32.8	29.0	Not corrected				17.9	18.6	6.3	29.8	
87R005					1	N	341.7		34.1										
87R004					3	N	333.9	35.2	39.0	45.4					15.7	32.3	7.7	41.0	
87R003			18.305	−66.875	3	N	347.3	63.3	40.0	76.5	348.8	57.6	35.4	79.0	6.5	52.7	7.7	41.0	
LA 1			18.3397	−66.677	3	N	332.5	46.6	35.6	64.4	333.7	44.8	32.0	66.7	9.6	42.2	7.7	41.0	270/8
LA 2			18.3469	−66.316	10	N	343.8	7.2	30.5	11.2	344.4	6.9	26.6	11.4	52.8	6.7	4.8	19.2	
LA 3			18.3353	−66.466	1	N	318.8		3.0		318.8		0.1						90/20
LA 4			Collection mean direction		25		341.2	7.3	32.8	10.9	341.8	7.2	30.1	11.2	18.5	6.9	**3.3**	**10.8**	
		Chattian [2] [3]	18.0314	−66.793	4	R, N*	342.7	20.6	17.0	38.1	342.5	20.9	19.0	37.9	20.9	20.6	6.9	34.2	90/20
UFO 1			17.9544	−66.904	9	R, N*	332.2	28.6	18.0	52.4	332.8	28.1	14.4	53.1	82.7	27.8	9.1	53.0	
UFO 2			Collection mean direction		13		329.0	11.5	27.7	18.7	326.3	13.2	33.8	19.2	11.9	12.5	**4.3**	**16.3**	
		Up. Rupelian-low. Chattian [1] [3]	See Reid et al. (1991)		5		340.3	19.6	41.1	24.2	Not corrected				19.2	17.9	6.3	29.8	
87R002					5		320.8	18.4	26.5	30.3					19.4	17.8	6.3	29.8	270/8
87R001			18.3519	−66.996	2	R, N*	313.2	81.3	46.8	73.1	316.1	74.1	44.0	76.6	19.5	60.0	9.1	53.0	
SEB 1		Siltstone	18.3556	−66.997	4	N	337.1	20.7	51.6	18.8	338.9	18.8	47.9	19.3	32.3	16.4	6.9	34.2	
SEB 2		Limestone	18.2983	−66.881	2	R, N*	322.0	13.5	32.0	20.4	317.3	15.2	39.7	19.5	14.4	14.1	5.0	20.5	
SEB 3		Siltstone	18.3381	−66.419	12	R, N*	308.7	12.6	41.0	15.6	311.2	12.0	38.5	15.8	16.2	11.1	4.4	17.1	
SEB 4			Collection mean direction		28		324.8	8.9	40.7	11.1	326.2	8.4	38.5	11.1	13.2	7.8	3.2	10.1	
	Volcaniclastic rock, Limestone	Late Cretaceous-Eocene	Collection mean direction		70						306.9	14.6	29.2	15.2	17.4	11.9	4.8	19.2	

Tectonics
10.1029/2022TC007706

Table 1
Continued

Sampling location							Geographic				Tectonic								
Puerto Rico	Lithology	Age	Lat.	Long.	Ni	Pol.	D	ΔD_x	I	ΔI_x	D	ΔD_x	I	ΔI_x	K	A95	$A95_{min}$	$A95_{max}$	Bedding
van Fossen et al. (1989)	Tuffite	43.4–30.6 My [4]	18.5285	−64.357	18	R*	312.8	7.8	29.3	12.3	318.5	6.9	14.9	13.0	26.4	6.9	3.8	13.3	270/20
	Microgabbro	30.7 ± 0.1 My [5]	18.341	−64.571	19	R	127.6	20.4	−25.6	34.1	132.9	19.8	−12.6	38.0	3.9	19.7	3.7	12.8	
UKVI			18.3363	−64.572															
NE1. NE2			18.3225	−64.596	14	R, N*	318.0	11.7	31.0	17.9	323.4	10.6	15.5	19.8	15.4	10.5	4.2	15.6	
			18.3733	−64.534	10	R, N*	343.4	30.5	39.0	39.5	346.4	28.1	19.7	50.6	4.0	27.6	4.8	19.2	
PE1			18.3761	−64.51	16	N	305.0	10.1	41.6	12.3	315.8	8.4	28.5	13.4	21.7	8.1	4.0	14.3	
PE2			Collection mean direction		52		316.0	6.0	37.5	8.1	324.2	5.2	22.0	9.1	15.8	5.1	2.5	6.7	
NO	Microgabbro	37.6 ± 0.1 My [5]	18.4194	−64.452	7	N	340.3	45.1	23.1	77.6	341.9	43.6	4.1	86.9	2.9	43.6	5.5	24.1	
SA			18.4415	−64.433	10	N	293.4	33.3	49.3	32.2	310.0	30.6	38.6	39.9	3.9	28.2	4.8	19.2	
CO			18.4323	−64.424	6	N	343.8	51.2	38.5	65.8	346.6	47.8	19.2	86.2	3.0	46.9	5.9	26.5	
			Collection mean direction		23		317.0	10.5	35.5	14.8	323.8	8.8	20.0	15.8	13.3	8.6	3.4	11.4	
FJ	Microgabbro	43.6 Ma ± 0.1 My [5]	18.4624	−64.417	13	N	303.5	13.5	48.1	13.8	317.2	9.5	35.0	13.5	22.3	9.0	4.3	16.3	
MI	Limestone	Tortonian to Messinian [6]	18.1672	−63.165	13	R, N*	355.4	6.6	32.0	10.0	355.3	7.1	36.9	9.7	39.6	6.7	4.3	16.3	87/5
CM			18.1603	−63.173	7	R, N*	18.0	12.9	22.3	22.5	21.0	12.4	17.0	22.9	25.3	12.3	5.5	24.1	347/10
			18.2004	−63.052	11	R, N*	355.9	12.0	39.0	15.6	359.2	12.7	42.2	15.3	16.5	11.6	4.6	18.1	37/5
RP			Collection mean direction		31		1.1	6.3	32.7	9.3	3.2	6.8	34.9	9.7	17.3	6.4	3.0	9.4	
	Limestone	Burdigalian to Langhian [6]	18.2633	−62.984	10	N	352.0	11.8	30.6	18.3	354.3	12.7	35.5	17.9	17.2	12.0	4.8	19.2	47/6
Anguilla			18.2239	−63.001	5	N	328.5	23.4	26.0	38.8	328.5	23.4	26.0	38.8	12.3	22.7	6.3	29.8	0/0
AA		Burdigalian [6]	18.1997	−63.036	7	R	336.9	12.0	16.0	22.3	336.7	12.3	20.0	22.1	25.9	12.1	5.5	24.1	72/4
WEC			18.2131	−63.075	5	R	333.2	20.9	29.8	32.7	328.4	24.3	40.9	30.1	12.9	22.2	6.3	29.8	92/13
AQ		Aquitanian [6]	18.2539	−63.017	4	R, N*	356.4	15.4	37.1	20.9	358.6	15.8	37.6	21.2	40.2	14.7	6.9	34.2	7/3
			Collection mean direction		31		342.0	7.0	27.7	11.3	342.3	7.7	32.2	11.5	13.5	7.3	3.0	9.4	

Tectonics
10.1029/2022TC007706

Table 1
Continued

Sampling location							Geographic				Tectonic								
Puerto Rico	Lithology	Age	Lat.	Long.	Ni	Pol.	D	ΔD_x	I	ΔI_x	D	ΔD_x	I	ΔI_x	K	A95	$A95_{min}$	$A95_{max}$	Bedding
CB	Limestone	Tortonian to Messinian [6]	18.0522	−63.137	14	R, N*	356.5	12.1	27.2	19.7	356.1	10.7	34.7	15.4	16.4	10.1	4.2	15.6	10/10
AL			18.0522	−63.137	4	N	343.7	15.1	42.0	18.2	352.0	12.9	24.9	21.8	54.4	12.6	6.9	34.2	294/21
SB			Collection mean direction		18		353.9	9.9	30.8	15.2	355.1	8.4	32.4	12.6	19.5	8.0	3.8	13.3	
KAT		Burdigalian [6]	18.0469	−63.128			No meaningful results. outlier												287/21
SA			18.0417	−63.118	2	R	169.1	21.8	−37.0	29.6	158.5	32.2	−53.1	27.4	92.2	26.3	9.1	53.0	107/19
		Burdigalian to Langhian [6]	18.1228	−62.975	3	R	326.5	28.8	31.2	43.9	321.3	29.8	37.9	39.6	21.0	27.6	7.7	41.0	102/10
Saint-Martin-Tintamarre			Collection mean direction		5		335.3	17.5	34.1	25.3	327.2	17.8	44.3	20.2	23.9	16.0	6.3	29.8	
CP															k	a95			
08E	Andesite	3–27 Ma [7]	18.0872	−63.034	4	N	326.2		14.5		333.3		53.3		8.4	28.1			
			18.1011	−63.022	2	R	164.8		24.2		162.5		−11.3		171.2	19.2			
10E			18.0789	−63.079	5	N	316.5		2.2		317.1		42.2		55.6	10.4			
11E–14E			18.0431	63.024	3	N	359.9		26.0		27.0		48.1		81.6	13.7			
TIB			18.0431	−63.027	2	N	350.5		26.6		17.5		54.2		896.2	8.4			
			18.108	−63.03	2	N	333.3		30.1		356.4		65.8		118.9	11.4			
			18.108	−63.03	1	R	147.3		17.1										
01E			18.0307	−63.032	3	N	324.2		28.2		336.3		67.1		18.8	29.3			
03E			18.0251	−63.048	3	R	139.5		34.4		138.7		−5.5		76.9	14.2			45/40 [7]
05E			18.0251	−63.048			No meaningful results. outlier												
16E			18.02	63.0671			No meaningful results. outlier												
18E			18.0195	63.0668	2	R	143.4		4.2		145.2		−35.3		17.1	64.6			
22E1			18.0222	63.0713	5	R	121.3		−13.2		113.3		−51.5		85.1	8.3			
22E2			18.0222	63.076	1	R	175.7		32.0										
28E			18.0472	63.0861	3	R	141.3		−13.9		145.2		−53.5		11.3	38.5			
29E			18.0472	63.0861			No meaningful results. outlier												
30E			18.0536	63.0714	7	R	134.2	13.6	16.0	25.4	134.1		−24.0		18.8	15.8			
31E			Collection mean direction		14		329.3	10.5	2.2	20.9	325.3	6.0	26.9	9.9	24.6	5.8	3.3	10.5	

Tectonics
10.1029/2022TC007706

Table 1
Continued

Sampling location							Geographic				Tectonic								
Puerto Rico	Lithology	Age	Lat.	Long.	Ni	Pol.	D	ΔD_x	I	ΔI_x	D	ΔD_x	I	ΔI_x	K	A95	$A95_{min}$	$A95_{max}$	Bedding
32E	Granodiorite	30–27 Ma [7]	18.1077	−63.031	5	N	325.8	6.0	−12.5	11.5	326.8	6.6	26.8	10.9	143.3	6.4	6.3	29.8	
33E			18.0141	−63.043	7	R	151.4	8.9	2.4	17.9	155.3	12.1	−35.7	16.9	29.2	11.4	5.5	24.1	
34E			18.1008	−63.031	3	R	133.7	26.3	−0.6	52.5	133.3	37.0	−40.5	45.9	14.5	33.6	7.7	41.0	
35E			18.0958	−63.038	4	R	131.5	17.7	12.4	34.0	131.5	15.6	−20.3	27.9	36.9	15.3	6.9	34.2	45/40 [7]
36E			18.0567	−63.029	6	R	149.6	15.6	29.0	24.8	147.9	13.6	−9.9	26.4	33.1	13.5	6.3	29.8	
38E			18.0142	−63.043	2	N	324.6	37.1	4.1	73.9	326.0	49.0	28.7	77.2	30.8	46.7	9.1	53.0	
			18.0261	−63.057			No meaningful results. outlier												
GR1			Collection mean direction		26		324.3	5.4	−10.3	10.5	333.9	15.2	40.7	19.0	9.1	14.0	4.2	15.6	
FT	Limestone, granodiorite	27–24 Ma [10]	Collection mean direction		126		334.0	3.2	13.7	6.2	335.7	3.6	13.5	6.9	17.5	3.6	1.9	4.6	
02E	Limestone	Aquitanian [8]	17.0997	−61.679			No meaningful results. outlier												1/1
04E		Chattian [8]	17.0919	−61.764			No meaningful results. outlier												340/18
15E			17.0919	−61.764			No meaningful results. outlier												1/1
19E			17.1286	−61.8			No meaningful results. outlier												315/5
21E		Rupelian to Chattian [8]	17.0028	−61.77			No meaningful results. outlier												320/13
	Lacustrial limestone	Priabonian to Rupelian [8]	17.0228	−61.758	20	N	332.8	13.2	24.7	22.4	338.0	14.9	18.6	27.1	18.0	14.6	5.5	24.1	320/10
			17.0436	−61.763	6	N	320.8	15.0	17.7	27.5	327.6	15.3	18.4	27.9	17.0	15.1	5.5	24.1	325/21
Saint-Barthelemy			17.1208	−61.88	4	N	326.9	18.8	19.1	34.0	331.2	20.7	11.9	39.9	36.9	20.6	7.7	41.0	304/17
	Siltstone		17.1308	−61.864			No meaningful results. outlier												230/8
Antigua			17.1406	−61.859	4	R	155.1	16.7	−11.9	32.1	160.0	17.5	−23.6	30.0	30.0	17.1	6.9	34.2	15/19
DB	Tuffite		17.0053	−61.765		N	340.9	6.5	12.9	12.4	337.5	5.8	13.7	11.1	457.2	5.8	7.7	41.0	156/14
PA 1 and 2			17.0836	−61.807			No meaningful results. outlier												317/22
PA 3	Granodiorite	Priabonian to Rupelian [8]	17.0119	−61.838	10	R	161.7	23.1	−13.9	43.8	163.6	23.7	−10.1	46.1	114.4	23.6	9.1	53.0	320/10 [8]
BU															k	a95			
PB	Andesite		17.0767	−61.831	4	R	155.3		−11.7		157.0		−8.9		96.3	9.4			
CH1 to 4			17.0253	−61.869	3	R	152.8		−26.5		157.4		−23.9		21.5	27.3			
CH 5	Basalto-andesite	27.0 ± 1.9 Ma [8]	17.0072	−61.768	4	N	339.6		27.3		339.6		27.3		26.7	18.1			156/14 [8]
FI			17.0044	−61.764			No meaningful results. outlier												
FJ	Dacite	29.8 ± 0.2 Ma [8]	17.0183	−61.798	13	N	355.2		30.5		359.4		24.4		93.9	4.3			320/10 [8]
CO	Andesite	35.3 ± 0.2 Ma [8]	17.0454	−61.894			No meaningful results. outlier												
TU 1	Basalto-andesite		17.0454	−61.894	5	N	6.6		35.7		10.5		29.2		6.8	31.6			
TU 2	Andesite		17.0454	−61.894	8	N	3.8		26.6		6.8		19.5		42.6	8.6			

Tectonics
10.1029/2022TC007706

Table 1
Continued

Sampling location							Geographic				Tectonic								
Puerto Rico	Lithology	Age	Lat.	Long.	Ni	Pol.	D	ΔD_x	I	ΔI_x	D	ΔD_x	I	ΔI_x	K	A95	$A95_{min}$	$A95_{max}$	Bedding
GR			Collection mean direction		24		333.9	6.1	22.2	10.7	335.2	5.5	20.2	9.8	31.1	5.4	3.4	11.1	
	Andesite	8.44 ± 0.12 Ma [9]	14.4916	−60.879	1	N	339.6		1.0		339.6		1.0		k	a95			Sub-horizontal [11]
BE			14.4702	−60.892	5	R	186.9		−11.5		186.9		−11.5		56.8	10.2			
SMA			14.5243	−61.052							No meaningful results. outlier								
NH1		8.76 ± 0.13 Ma [9]	14.6642	61.0234							No meaningful results. outlier								
NH2		8.98 ± 0.18 Ma [9]	14.5485	−61.05	5	R	158.6		−6.2		158.6		−6.2		83.6	8.4			
DAC*			14.5499	−61.054							No meaningful results. outlier								
AND 1			14.5488	−61.058	5	N	0.1		38.1		0.1		38.1		71.4	9.1			
AND 2			14.5368	−61.043	5	N	353.8		3.2		353.8		3.2		69.5	9.2			
AND 3			14.5334	−61.047	4	N	344.1		27.0		344.1		27.0		417.2	4.5			
		9.23 ± 0.14 Ma [9]	14.5154	−60.945							No meaningful results. outlier								
Martinique			14.4764	−60.939	2	R	152.9		−16.8		152.9		−16.8		253.6	15.8			
ML			14.4726	−60.936	5	R	164.9		−11.1		164.9		−11.1		256.9	4.8			
AS		9.89 ± 0.12 Ma [9]	14.5236	−60.896	5	N	338.9		24.5		338.9		24.5		46.5	11.3			
MA		11.98 ± 0.39 Ma [9]	14.7106	−60.934	2	N	356.6		21.8		356.6		21.8		32.2	45.6			
SoB			14.7054	−60.936	2	N	354.3		23.2		354.3		23.2		231.6	16.5			
TP			14.6463	−60.939							No meaningful results. outlier								
CL			14.6463	−60.939	1	N	0.9		−18.8		0.9		−18.8		36.8	15.4			
BM			14.5762	−60.857	5	N	344.0		15.8		344.0		15.8		106.2	7.5			
CU			14.5721	−60.894	7	N	0.6		44.3		0.6		44.3		25.1	12.3			
MJ		16.12 ± 0.23 Ma [9]	14.52	−60.844	3	N	3.8		23.1		3.8		23.1		67.4	15.1			
TC			14.52	−60.844	1	R	154.5		−32.7		154.5		−32.7						
CG			14.6055	−60.955	5	N	355.8		14.5		355.8		14.5		396.9	3.9			
JJ			14.5844	−60.857	7	R	146.2		11.4		146.2		11.4		141.0	5.1			
SZ			14.5623	−60.927	5	R	178.4		−3.6		178.4		−3.6		19.3	17.9			
JC			14.5966	−60.897	7	N	345.1		10.7		345.1		10.7		161.7	4.8			
GF			Collection mean direction		18		349.4	5.5	18.5	9.9	349.4	5.5	18.5	9.9	42.4	5.4	3.8	13.3	

Tectonics
10.1029/2022TC007706

Table 1
Continued

Sampling location							Geographic				Tectonic								
Puerto Rico	Lithology	Age	Lat.	Long.	Ni	Pol.	D	ΔD_x	I	ΔI_x	D	ΔD_x	I	ΔI_x	K	A95	$A95_{min}$	$A95_{max}$	Bedding
FM1	Andesite	23.08 ± 0.39 Ma [9]	14.4849	−60.82	1	N	325.9		16.1		325.9		16.1		k	a95			Sub-horizontal [11]
FM2			14.4879	−60.82	5	N	4.5		23.4		4.5	10.1	23.4	17.5	41.5	12.0			
PC			14.4867	−60.826			No meaningful results. outlier												
TM			14.4744	−60.833	5	R	191.8		−10.9		191.8	6.1	−10.9	11.9	61.7	9.8			
PM1			14.4724	−60.833			No meaningful results. outlier												
PM2			14.4683	−60.827	4	N	351.7		11.5		351.7	9.2	11.5	17.8	70.1	11.1			
MEL		25.46 ± 0.4 Ma [9]	14.3973	−60.877	3	N	333.9		27.2		333.9	6.9	27.2	11.3	370.6	6.4			
PR			14.3973	−60.877	3	N	324.0		44.6		324.0	26.1	44.6	29.3	33.0	21.8			
LEN			14.4501	−60.863	4	N	340.3		16.3		340.3	7.3	16.3	13.6	90.5	9.7			
BS		25.2 ± 0.4 Ma [9]	14.7689	−60.89	4	N	351.5		28.2		351.5	7.6	28.2	12.3	135.3	7.9			
		23.39 ± 0.34 Ma [9]	14.7541	−60.911	5	R	160.3		−23.9		160.3	5.2	−23.9	9.0	129.7	6.7			
TA			14.7541	−60.914	5	R	191.3		−40.4		191.3	12.2	−40.4	15.3	29.6	14.3			
VM			14.754	60.9092	5	R	203.4		−2.3		203.4	11.5	−2.3	22.9	25.2	15.5			
OL			Collection mean direction		11		351.3	12.3	23.3	21.1	351.3	12.3	23.3	21.1	15.5	12.0	4.6	18.1	
SK	Limestone	Aquitanian to Burdigalian [9]	14.5025	−60.823			No meaningful results. outlier												Sub-horizontal [11]
CC		Chattian [9]	14.7554	−60.938			No meaningful results. outlier												
TT	Basalt	Middle Eocene	Collection mean direction		15						1.6	11.9	21.2	15.3	13.7	10.7	4.1	14.9	

Note. In blue: published paleomagnetic data from van Fossen et al. (1989), Reid et al. (1991), Speed et al. (1997), and Philippon, van Hinsbergen, et al. (2020). The St-Barthélemy collection is composed of directions interpreted from specimens of upper Eocene limestones and of Oligocene granodiorite. We compiled these directions in one Oligocene collection as the authors conclude a remagnetization of the Eocene limestones due to the pluton intrusion. Lat = Latitude; Long = Longitude; Ns = number of sampled specimens; Nd = number of demagnetized specimens; Ni = number of interpreted ChRM Directions. Pol. = Polarity; * = normalized sampling location; D = Declination, ΔD_x = Error on declination following Butler (1992); I = Inclination; Δi_x = Error on inclination following Butler (1992); a95 = cone of confidence assuming Fisherian distribution of paleomagnetic directions; k = Fisher (1953) precision assuming Fisherian distribution of paleomagnetic directions; A95 = cone of confidence assuming Fisherian distribution of virtual geomagnetic poles; K =Fisher (1953) precision assuming Fisherian distribution of virtual geomagnetic poles; A95min, max = Deenen et al. (2011) n-dependent reliability envelope; Bedding : strike/dip. [1] Ward et al. (2002), [2] Renken et al. (2002), [3] Ortega-Ariza et al. (2015), [4] Helsey (1960), [5] Schrecengost et al. (2009), [6] Cornée et al. (2021), [7] Noury et al. (2021), [8] Montheil et al. (2023), [9] Germa et al. (2011), and [10] Philippon, Cornée, et al. (2020). For the van Fossen et al. (1989) and the Reid et al. (1991) data sets the statistical parameters ΔDx, Δix, and A95min,max were not available in the published data and were obtained by parametric sampling with the paleomagnetism.org tool (Koymans et al., 2016, 2020). K and a95 are used for lavas sampling locations to estimate the direction dispersion due to sampling or measurement errors at a sampling location level. K, A95, A95min, and A95max are used for the sediments and granodiorite sampling location and collection means to check for pole dispersion due to paleosecular variation.

Figure 4. Example of sampling locations in (a) limestones sequence of Cupecoy Beach, in Saint-Martin (sampling location: CP); (b) Andesite of Bendal Carry, Antigua (sampling location: BE), and (c) Granodiorite containing mafic enclaves of Fallen Jerusalem, British Virgin Islands (sampling location: FJ).

Rankin, 2002) (Figures 2 and 3). This sequence forms an arch with the northern flank having a mean dip of 8° toward the north and the southern flank having a mean dip of 20° toward the south (Mann et al., 2005; van Gestel et al., 1998) (Table 1). The paleomagnetic sampling locations were collected along two E-W trending transects on the northern and the southern flanks of the island (Figure 3). In total, 237 core specimens were sampled from 18 locations, two within silts and 16 within limestones (Table 1).

In the British Virgin Islands, we targeted mafic, fine-grained enclaves in granodiorites that are exposed on a series of small islands as well as on the larger Virgin Gorda Island, and are interpreted to be part of three large, middle Eocene to lower Oligocene granodioritic plutons (Schrecengost et al., 2009; Smith et al., 1998) (Figures 2 and 3). A total of 210 cores were sampled from 10 locations: one in the Virgin Gorda pluton, three in the Bath pluton, five in the Salt pluton, and one location in volcaniclastic rocks of the Necker Fm. On Necker Island, that is interpreted to represent effusive equivalents of the plutonic rocks (Helsey, 1960) (Table 1 and Figures 2 and 3). The close vicinity of these non-metamorphic volcano-sedimentary rocks of Necker Island and the plutonic and metamorphic rocks of Virgin Gorda makes it likely that a large (normal) fault is present between these islands, although this has not been documented so far (Wilson et al., 2019).

In Saint-Martin we collected Eocene to lower Oligocene magmatic samples interbedded in, or intruding, the ~40° SE dipping Eocene volcaniclastic sequences (Dagain et al., 1989; Noury et al., 2021). These include andesitic lava flows and sills from which we collected 35 cores from 6 lava and 20 oriented blocks from 10 lava (Figures 2 and 3 and Table 1) and lower Oligocene granodioritic plutons that intruded the Eocene series. Thermochronological data indicate a rapid cooling of the plutons between 28.4 and 29.5 Ma (i.e., below 200°C, Noury et al., 2021), which we assume as the age of the characteristic magnetization. From these plutons we sampled 38 cores from 7 locations (Table 1 and Figures 2 and 3).

In Saint-Martin, Tintamarre and Anguilla, we targeted a Miocene to Pliocene limestone sequence (Cornée et al., 2021). In Saint-Martin, we collected 70 cores from five sampling locations. In Tintamarre, we sampled 15 oriented blocks from one location. In Anguilla, we sampled 207 cores from eigth sampling locations.

In Antigua, we collected upper Eocene to lower Oligocene magmatic and volcaniclastic units (Basal Volcanic Suite and the Central Plain Group), and the overlying upper early Oligocene–lower Miocene limestones (Antigua Formation) (Montheil et al., 2023 and references therein). The whole sequence is gently dipping (5°–10°) toward the North-East (Table 1). The magmatic units include andesitic lavas, dacitic domes, a granodiorite, and basaltic andesite to rhyolitic dykes that have been recently dated from 35.3 to 27.0 Ma (Montheil et al., 2023). Evidence for a hydrothermal event has been observed in the three units of Antigua leading to partial or complete rejuvenation of volcanic rocks between 10 and 20 Ma according to $^{40}Ar/^{39}Ar$ spectra (Montheil et al., 2023). In total, we sampled 60 cores from eight lava, 11 cores from a granodioritic pluton, 21 cores from two tuffs locations, 71 cores from five locations in siltstones and 65 cores from five locations in limestones (Table 1 and Figures 2 and 3).

Finally, the island of Martinique consists of volcanic sequences spanning the lower Oligocene to Recent, divided into three formations: the lower Oligocene to lower Miocene Sainte-Anne and La Caravelle Fm., the middle to upper Miocene Vauclin Pitault Fm. and the Pliocene to Present-day volcanic units of the active Lesser Antilles arc (Germa et al., 2011). These formations are mainly composed of andesitic lava flows and associated breccia. In places, the volcanics are interbedded with patches of limestones (Macabou Fm., lower Miocene; La Caravelle Fm., upper Oligocene; Andréïeff et al., 1988). We collected 73 cores from 14 Oligocene lava, 128 cores from 23 middle to upper Miocene lava and 63 cores from the interbedded limestones (Table 1 and Figures 2 and 3).

3.1. Paleo-Direction Determinations

We investigated the magnetic remanence of samples with thermal (TH) demagnetization and alternating field (AF) demagnetization using the robotized 2G SQUID demagnetization protocols in the paleomagnetic laboratory at the University of Montpellier, France, and alternating field (AF) demagnetization using the robotized 2G SQUID demagnetization protocols (Mullender et al., 2016) in the paleomagnetic laboratory "Fort Hoofddijk" at Utrecht University, the Netherlands. Two pilot samples per sampling location were treated in a null magnetic field environment by stepwise AF demagnetization. TH pilot demagnetization was undertaken when the AF demagnetization diagrams showed erratic behavior. For each collection, the demagnetization treatment giving the clearest demagnetization behavior was selected, from which the characteristic remanent magnetization was interpreted (ChRM). Variable field increments (4–20 mT), up to 140 mT were selected depending on pilot sample demagnetization behavior. Stepwise TH demagnetization was carried out with a laboratory-built furnace with 50°–100° increments from ambient temperature up to 680°C. Magnetic remanence was measured at each heating step. Special care was taken in the analysis of weakly magnetized limestones (10^{-10} to 10^{-12} A.m.^{2}). For these specimens, sample holders were cleaned with an ultrasonic bath for 10 minutes, dried with compressed air and demagnetized under a field of 120 mT. When the quality of the limestone core sample was sufficient, two specimens per core were analyzed.

Representative samples for lithologies and demagnetization behavior were selected for rock magnetic analysis and the magnetic mineralogy for each lithology was determined with susceptibility variation during heating (K-T) (Figures S1A and S1B in Supporting Information S1). ChRM directions were interpreted by means of the principal component analysis (Kirschvink, 1980). Demagnetization data were plotted in Zijderveld diagrams (Zijderveld, 1967) and stereographic projection with the online Paleomagnetism.org software package (Koymans et al., 2016, 2020). Examples of demagnetization diagrams are presented in Figure 4. Interpreted ChRM directions are grouped per sampling location to spot outlier sampling locations. We check the consistency of Virtual Geomagnetic Poles (VGP) dispersion with the predicted values for paleosecular variation (Cromwell et al., 2018) and quantify the dispersion with the precision parameter K (Fisher, 1953). We also investigate if the collection of VGPs falls within the $A95_{min\text{-}max}$ n-dependent confidence envelope of Deenen et al. (2011). Finally, the paleomagnetic data collected from sedimentary rocks may suffer from inclination shallowing, and direction-based methods to correct for this effect require collections of 80–100 spot readings of the magnetic field (e.g., Tauxe & Kent, 2004; Vaes et al., 2021). Our collections are typically smaller than that, and we do not correct our data for inclination shallowing. This does not influence the declination that we use for our rotation analysis and the paleomagnetic inclination is not of direct importance for our study. As the Caribbean plate has remained stable around its modern latitude since the Eocene (e.g., van Hinsbergen et al., 2015), we only check whether the inclination is not strongly deviated from shallow-down (normal polarity) or shallow-up (reversed polarity). All inclinations of the ChRM collections that we interpreted below fall within the range expected from the global Apparent

Polar Wander Path (APWP) in Caribbean coordinates (S.I. Figure S2), suggesting that bedding tilt was properly corrected, and that inclination shallowing is not of major concern for the sedimentary collections.

4. Results

4.1. Puerto Rico

4.1.1. Paleomagnetic Interpretations

Intensities of the Natural Remanent Magnetization (NRM) of the limestone collections (Table 1) ranges from 0.02 to 0.9 mA/m. For the silt samples (Table 1), the NRM varies from 0.4 to 25 mA/m. The Alternaltive Field (AF) and thermal (TH) demagnetization behaviors are noisy due to the low intensity of the magnetization of the limestones, and perhaps due to the presence of coarse multi-domain grains in the siltstones. About 35% of the specimens show consistent demagnetization behavior. From these, a stable component is recognized in the range of 30–80 mT or 300–540°C that typically decays toward the origin of the Zijderveld diagram (Figures 5a and 5b). This component is interpreted as the Characteristic Remanent Magnetization (ChRM). It is recognized in both normal and reverse polarities and deviates counterclockwise (CCW) from north in Oligocene rocks (Figure 6a and Table 1). The range of TH demagnetization and KT experiments suggest that the ChRM is carried by magnetite or titano-magnetite (Figure S1 in Supporting Information S1). Chemical mineralogic transformation is observed during the TH treatment for the 540 and 600°C heating steps (Figure 5c). At sampling locations CIB, SEB2, and UFO2, a non-demagnetizing component is recognized at high-coercivity steps leading to great circle trajectories (Figure 5c). We use these great circles in combination with directions estimated from specimens with an isolated ChRM component to determine a most likely ChRM (McFadden & McElhinny, 1988). From sampling locations AYA1 and MB1, no meaningful magnetic components were isolated. High intensities are observed for the limestones of the AGU, LA3, and UFO2 sampling locations. AF diagrams of these specimens show a component that quickly demagnetizes from 0 to 20 mT. The associated interpreted directions are highly dispersed, which we interpret as a (possibly lightning-induced) overprint. In addition, a soft overprint aligned with the present geomagnetic field direction is recognized (Figure 5b).

4.1.2. Data Collections

We combine the ChRM directions of this study with the published directions of Reid et al. (1991) as both data sets show consistent directions per sampling location (Figures 6a and 6b) and were sampled in the same stratigraphic units. The Puerto Rico directions are divided into five collections of different ages: three upper Oligocene collections, one lower Miocene collection and one middle to upper Miocene collection (Table 1 and Figure 7). We also include in our data set the late Cretaceous to Eocene collection of van Fossen et al., 1989 and the Pliocene collection of Reid et al. (1991) (Table 1 and Figure 7). The collections have A95 values that fall within the reliability envelope of Deenen et al. (2011) (A95 min < A95 < A95max), showing that the data scatter may be straightforwardly explained by PSV alone and that non-PSV contributions to the scatter (e.g., within-collection rotations, measuring errors) are minor. We interpret the ChRM collections as primary magnetizations, and the coherence of the data from different sampling locations shows that Puerto Rico may be considered (part of) a paleomagnetically coherent block without internal rotations.

4.2. British Virgin Islands

4.2.1. Paleomagnetic Interpretations

NRM intensities of the mafic enclave specimens vary between 55 and 620 mA/m. The NRM of the Necker volcaniclastic rocks is lower, with values ranging between 0.1 and 8.2 mA/m. Overall, AF and TH demagnetization diagrams reveal stable demagnetization behavior. At sampling locations RP, PE1, FJ and NE1 a non-demagnetizing component (probably carried out by hematite), is observed for high-coercivity steps (Figure 5e) and sometimes completely overprints the ChRM. At sampling locations RP, MI, FJ, high intensities (300–2230 mA/m) are recognized at low coercivity steps. This component demagnetizes quickly and is interpreted as lighting strike overprints. Noisy diagrams, for example, at sampling location CM or CO, are associated with the presence of multidomain grain (MD), recognized in KT experiments (Figure S1 in Supporting Information S1). Two components are typically recognized in the remaining samples (Figure 5d). The first one is a north-directed component that ranges from 0 to 20 mT and 25–250°C that we interpret as a present-day field overprint. The second one shows normal and reverse polarities, decays toward the origin of the Zijderveld diagram, and is recognized at medium to high coercivity steps (10–100 mT) or at medium to high temperature

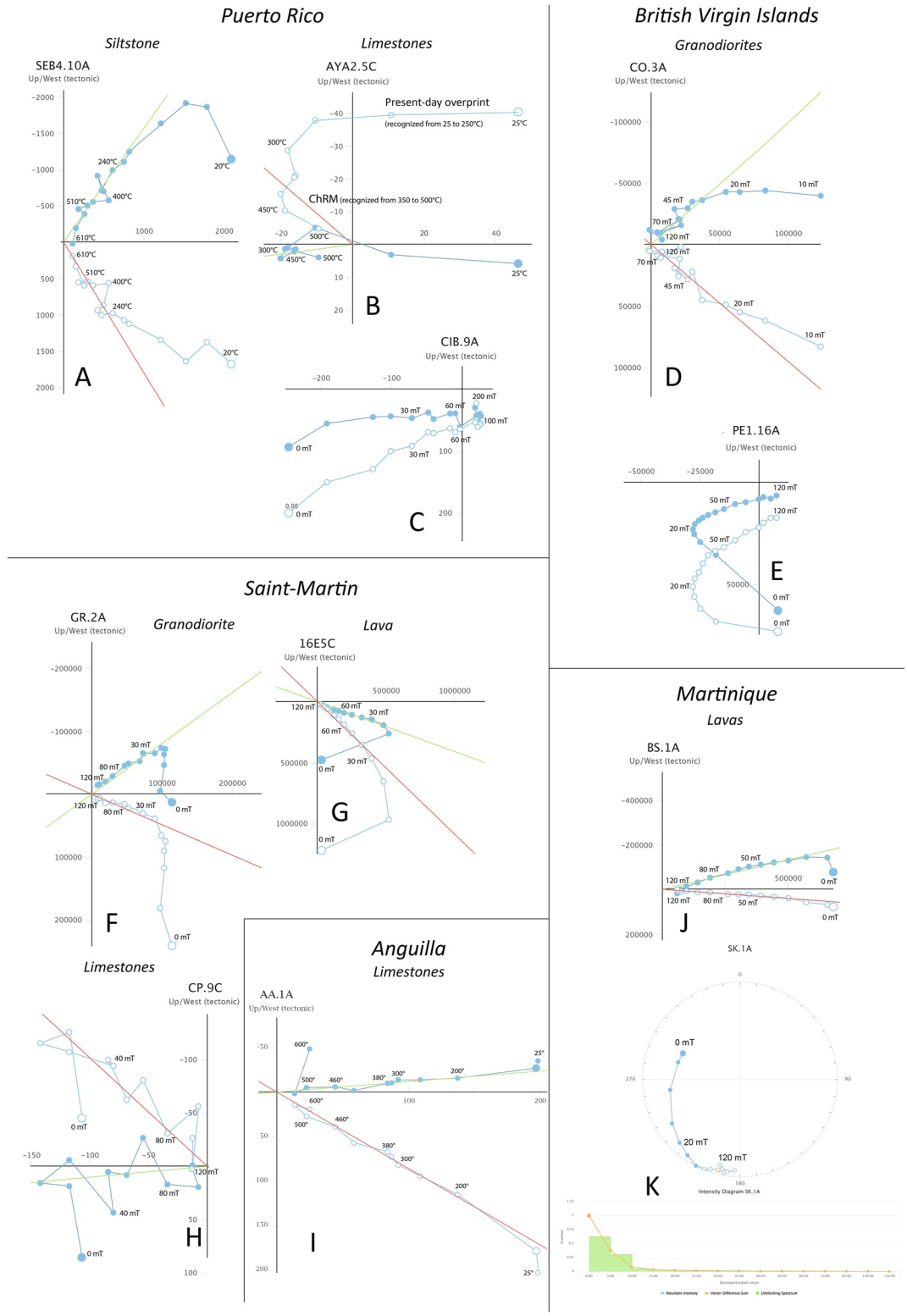

Figure 5. Example of Zijderveld diagrams, equal area stereographic projection and intensity diagrams of the granodiorite, lavas, volcaniclastics, siltstones and limestones specimens. Blue dots: horizontal projection, white dots: vertical projection. In the stereographic projections, the blue dots represent a direction pointing down and the white dots a direction pointing up.

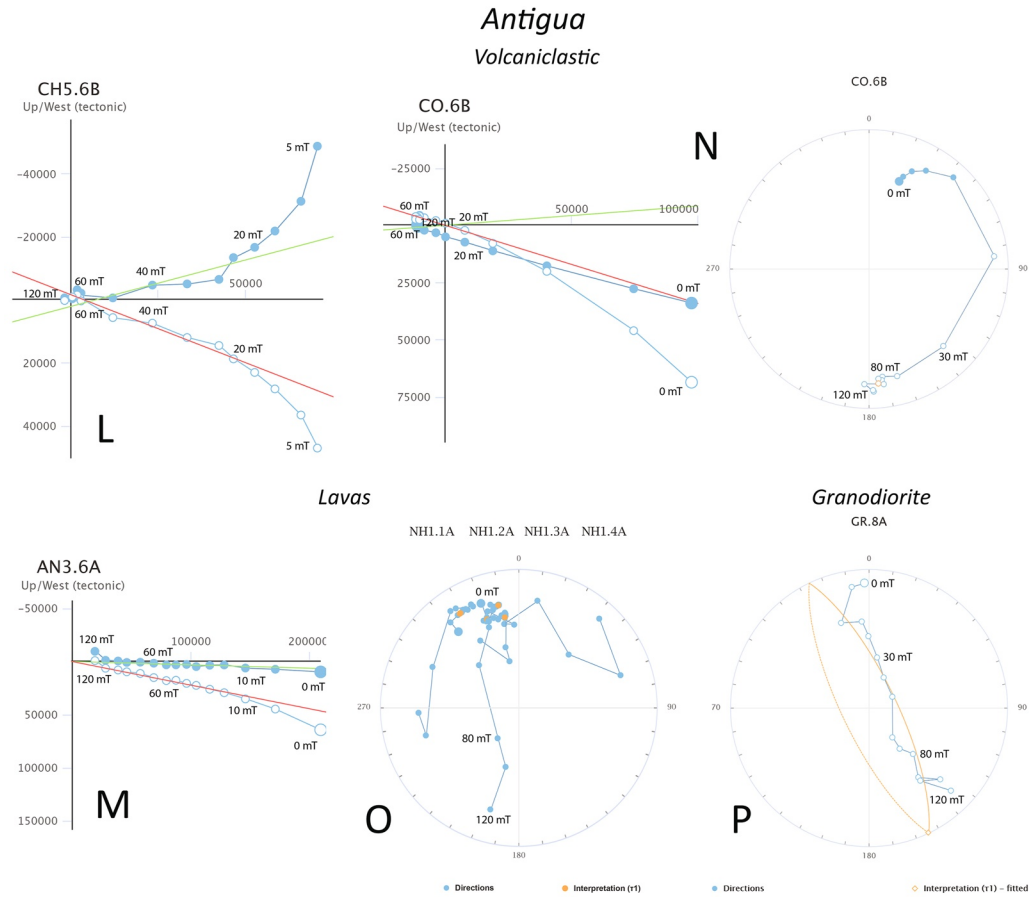

Figure 5. (Continued)

(330–600°C) with declinations typically deviating counterclockwise from north. We interpret this component as the ChRM. The blocking temperature and KT experiment indicates that the magnetic components are carried by multidomain (MD) to pseudo single domain (PSD) grains of magnetite in the mafic enclaves specimens and by titano-magnetite in the volcaniclastic specimen of Necker Island (Figure S1 in Supporting Information S1).

4.2.2. Data Collections

The ChRM directions are compiled per pluton (Virgin Gorda, Bath, and Salt plutons) and for the Necker Formation volcaniclastics. These collections pass the Deenen criterion. Reversals are recognized for the Salt pluton, which is possible given its age (30.7 ± 0.1 Ma, Schrecengost et al., 2009) that overlaps the C12n and the C11r chron (Ogg, 2020). A positive reversal test was performed on this collection (Figure S3A in Supporting Information S1). The Virgin Gorda and Bath plutons mainly contain normal polarity that is consistent with their age (43.6 ± 0.1 and 37.6 ± 0.1 Ma, Schrecengost et al., 2009) that falls into the normal C20n and C17n chron. The age of the BVI plutons ranges from the late Eocene to the early Oligocene (Figure 2 and Table 1). The latest pluton is dated at 30 Ma (Schrecengost et al., 2009) and could potentially have remagnetized the Virgin Gorda and Bath plutons. Nevertheless, we do not observe indications of a remagnetization in the paleomagnetic data set. We thus consider the ChRM directions primary and coeval with the age of the plutons.

4.3. Saint-Martin and Tintamarre

4.3.1. Paleomagnetic Interpretations

The NRM intensity of the lavas and granodiorites of Saint-Martin ranges from 4 to 1,500 mA/m. All magmatic rock samples were demagnetized by means of AF treatment and diagrams show stable demagnetization behavior except for samples from locations 15E and FT for which we suspect multidomain magnetic carriers. KT experiments

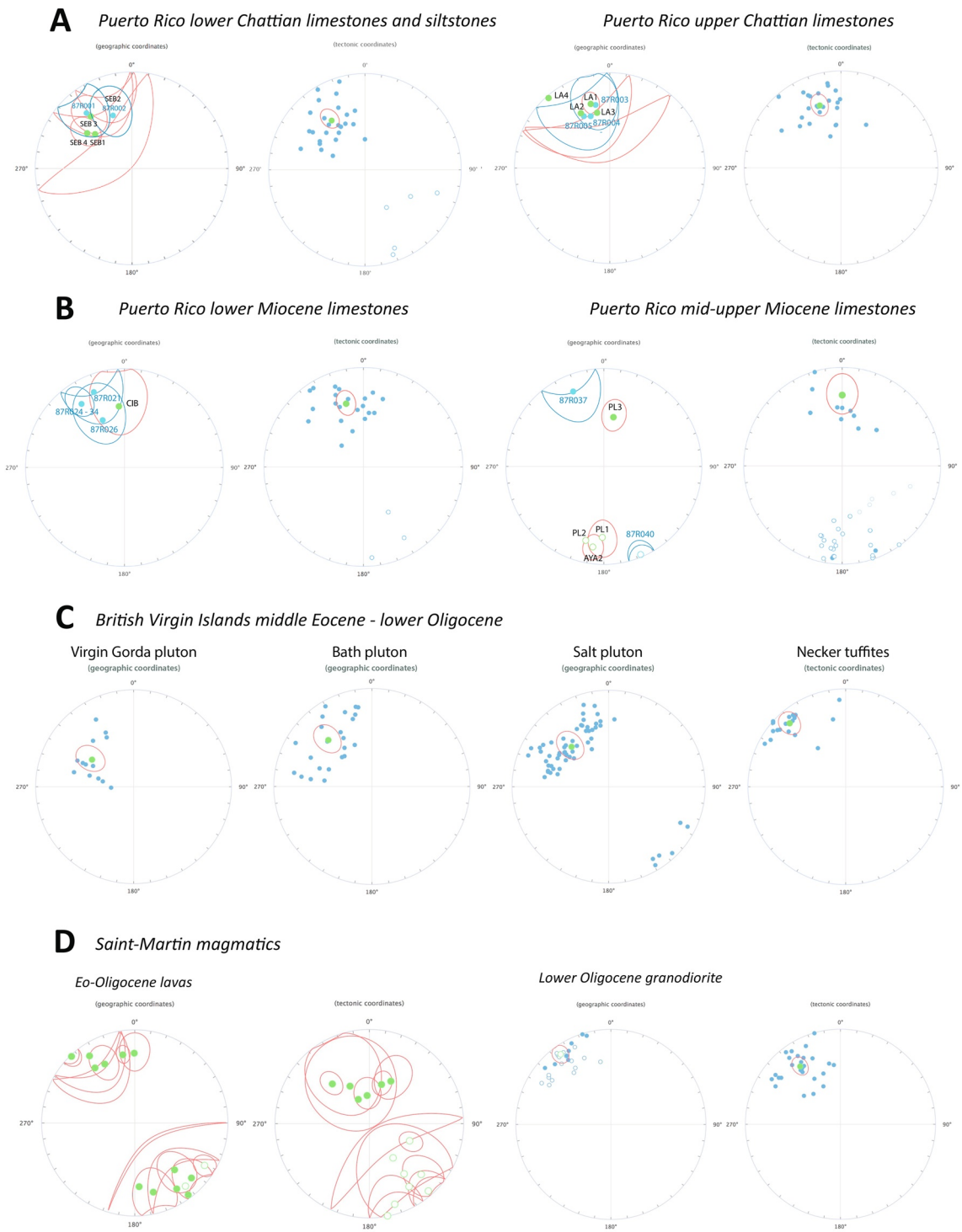

Figure 6. To the left: Stereographic projections of the mean direction per sampling location and confidences ellipses. (a and b) In blue, mean direction per sampling location from Reid et al. (1991). The mean direction is consistent with the one of this study. The confidence ellipses of the middle to upper Miocene sampling locations are not overlapping but the directions per specimen are consistent when combined and the collections passes the quality criteria of Deenen et al. (2011). To the right: stereographic projections of the directions and mean normalized direction (green dot) and confidence ellipse (red line) of the paleomagnetic collections.

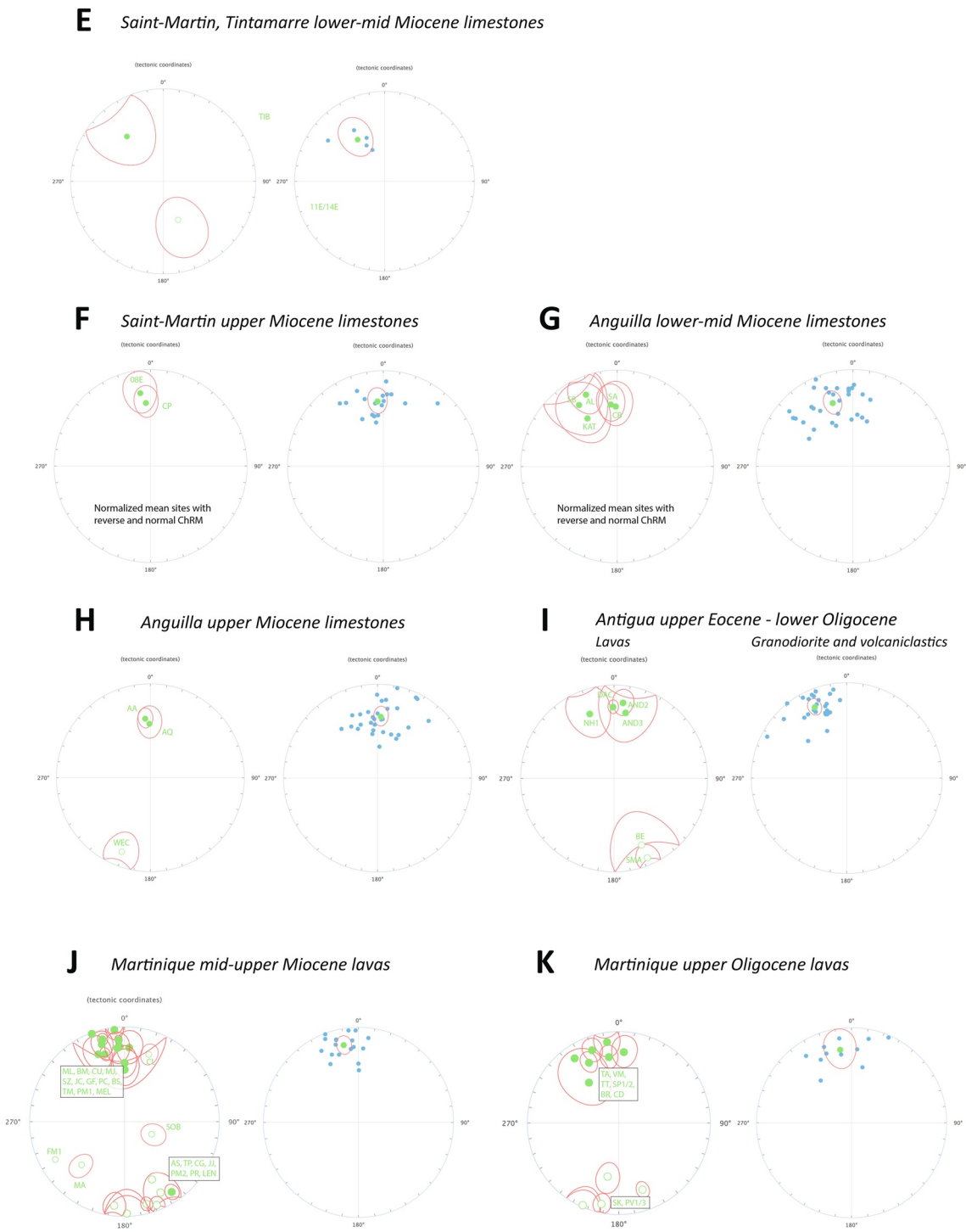

Figure 6. (Continued)

indicate that the magnetic mineralogy is dominated by MD to SD magnetite (Figure S1 in Supporting Information S1). A north-oriented normal component is recognized at low coercivity steps (0–20 mT) and interpreted as a present-day field overprint (Figures 5f and 5g). Reversed and normal polarity components decaying toward the origin are recognized in the range of 10–100 mT treatment and interpreted as the ChRM (Figures 5f and 5g). Some locations had high-intensity magnetizations that in the first steps demagnetized quickly and yielded erratic directions (locations 15E, 19E), which we interpret as lightning-induced magnetizations. For some specimens

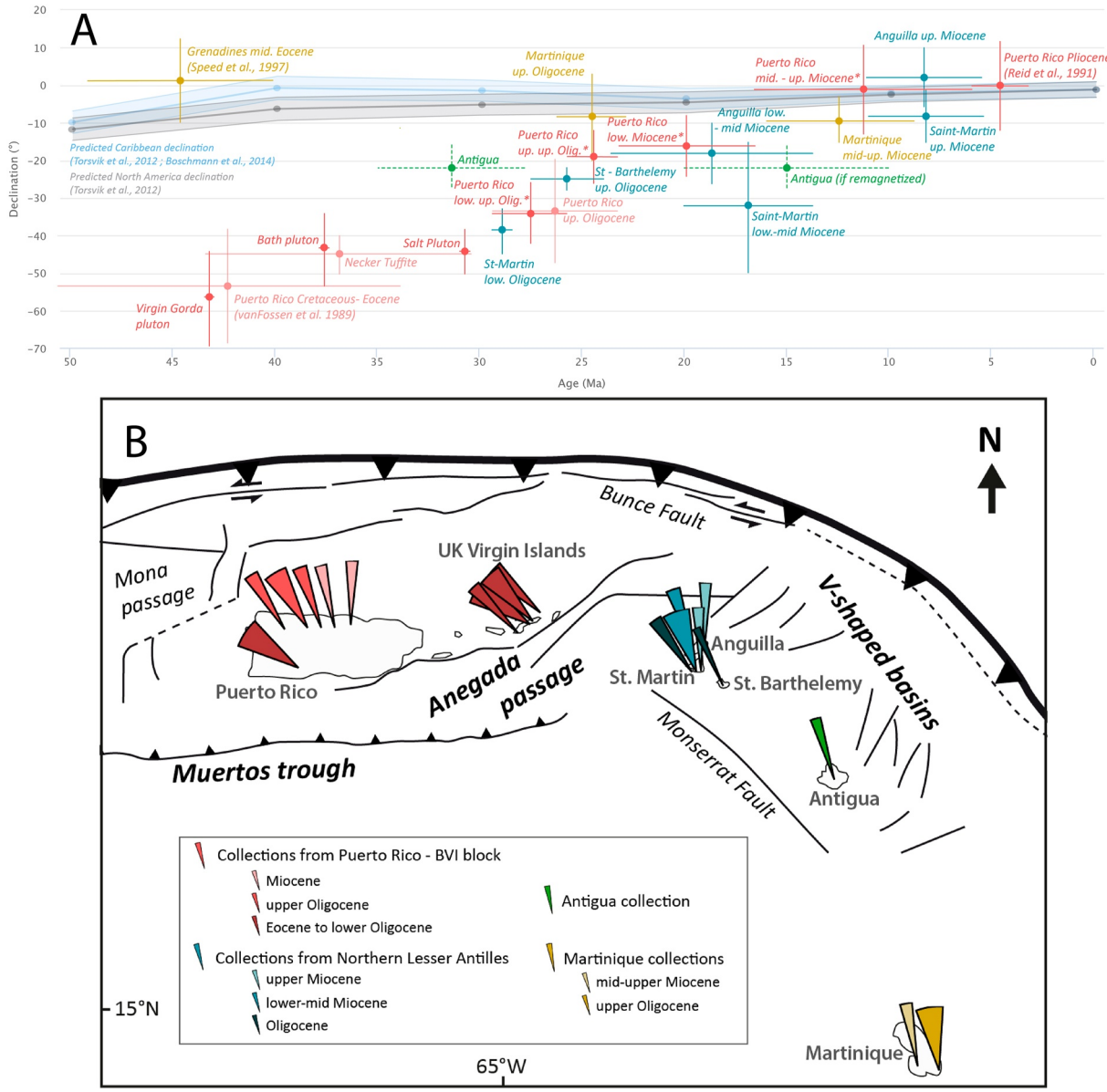

Figure 7. (a) mean declination of the paleomagnetic collection compared to age with declination and age uncertainties. In red: collection from the islands of the Puerto Rico-Virgin Island block. The lighter red colors outline collections whose stratigraphic age is uncertain. In Puerto Rico, this age uncertain collection was not used for relative rotation estimates to optimize the time framing of the paleo-rotation estimates. *: collection containing a combination of direction from this study and from Reid et al. (1991). In blue: collection from the islands of the Northern Lesser Antilles block. In green: Antigua collection, the dotted lines are used to indicate that the age of magnetization is uncertain. In yellow: Martinique collections. (b) Simplified structural map of the north-eastern Caribbean and mean declination with uncertainties (ΔDx) per paleomagnetic collections.

at sampling location 04E, 16E, 36E, FT, a component does not demagnetize at high magnetizations with in the first steps the demagnetization is quick and yields erratic directions (locations 15E, 19E), which we interpret as lightning-induced magnetizations. For some specimens at sampling location 04E, 16E, 36E, FT, a component does not demagnetize at high coercivity steps. Alteration features were observed at those sampling locations indicating that this component is probably carried by hematite formed during secondary alteration processes.

The NRM of the limestones vary from 0.01 to 1 mA/m. AF and TH demagnetization diagrams are noisy due to the low intensity of magnetization. A normal, northerly soft component is observed in most of the specimen and is associated with a present-day field overprint (Figure 5i). A hard component decaying toward the origin was identified from 10 to 80 mT in AF and from 250° to 550°C in TH (Figure 5h) in both normal and reversed polarities that we interpret as the ChRM. AF demagnetization was successful for most of the specimens and

TH demagnetization diagrams indicating a drop in intensity around 450°C suggesting that the ChRM is carried by magnetite and titanomagnetite. KT experiments were not successful in limestones samples due to an initial susceptibility magnitude close to the device noise level (Figure S1 in Supporting Information S1).

4.3.2. Data Collections

We averaged the directions for each lava sampling location and compiled these directions into one collection. The mean normalized direction in geographic coordinates is $D \pm \Delta D_x = 329.25 \pm 10.48$; $I \pm \Delta I_x = 2.17 \pm 20.94$ (Table 1). When corrected by the mean 40°SE dipping bedding, the mean normalized direction is $D \pm \Delta D_x = 325.3 \pm 6.0$; $I \pm \Delta I_x = 26.9 \pm 9.9$ (Table 1). As the age of the lavas, that are estimated either as Oligocene intrusive rocks (Noury et al., 2021) or mid Eocene lava flows interbedded within the sedimentary sequence (Dagain et al., 1989), is uncertain, it is not possible to correct the lava specimen tilt according to the local Eocene sedimentary sequence dip. Consequently, the nature of the lava's magnetization (primary or remagnetized) cannot be tested by a fold test.

For the granodiorite specimens, the mean direction is $D \pm \Delta D_x = 326.0 \pm 5.7$; $I \pm \Delta I_x = 30.0 \pm 8.9$ (Table 1). When corrected by the mean 40°SE dipping bedding, the mean normalized direction is $D \pm \Delta D_x = 333.9 \pm 15.2$; $I \pm \Delta I_x = 40.7 \pm 19.0$ (Table 1). For granodiorite specimens, we infer a magnetization age that is equal to the age of the plutons, that is, 28.4 to 29.5 Ma (Noury et al., 2021). Both collections pass the Deenen et al. (2011) criterion showing that there is no reason to suspect significant other contributions to the data scatter than PSV (Table 1 and Figures 6 and 7). In geographic coordinates, the mean inclination of the granodiorite and the lavas are negative or close to 0 (Table 1) which is not expected for this latitude. When corrected for the 40°SE dip, the mean inclination is positive suggesting that the granodiorite and lavas were tilted together with the Eocene sedimentary sequence, as suggested by Noury et al. (2021). A positive reversal test was performed on a collection comprising both the lava mean directions and the granodiorite collection (Figure S3B in Supporting Information S1). This suggests that either the lavas were remagnetized by the Oligocene granodiorite intrusions, similar to what was previously shown for nearby St. Barthelémy (Philippon, van Hinsbergen, et al., 2020) or that (part of) the dip of the lavas is primary, on the flanks of a stratovolcano.

For the limestones, we averaged the directions in two collections. A lower to mid Miocene collection that has a mean direction of $D \pm \Delta D_x = 327.2 \pm 17.8$; $I \pm \Delta I_x = 44.3 \pm 20.2$ and an upper Miocene collection that has a mean direction of $D \pm \Delta D_x = 355.1 \pm 8.4$; $I \pm \Delta I_x = 32.4 \pm 12.6$ (Table 1). In Saint-Martin and Tintamarre we interpret the stratigraphic age as the magnetization age.

4.4. Anguilla

4.4.1. Paleomagnetic Interpretations

The NRM of the limestones range from 0.02 to 1.2 mA/m. Due to the low intensity of magnetization, AF and TH demagnetization diagrams are of poor quality. We manage to interpret a consistent ChRM component from 20 to 100 mT in AF and from 250° to 550° in TH (Figure 5i) in both normal and reverse polarities and that is CCW rotated for some sampling localities. Upon thermal demagnetization we observed a drop of the intensity around 500° suggesting that the ChRM is carried by magnetite and titanomagnetite. The presence of goethite is suspected at sampling locations KAT and WEC leading to an absence of demagnetization by AF techniques and a demagnetization around 100–150°C in TH analysis. A soft component aligned with the present geomagnetic field direction is observed in most of the specimen (Figure 5i).

4.4.2. Data Collections

In Anguilla, we average the data set in two collections: the first comprises the lower to mid Miocene sampling locations, the second comprises the late Miocene sampling locations (Table 1 and Figures 6 and 7). Both collections pass the Deenen criterion (A95 min < A95 < A95max). In Anguilla we interpret the stratigraphic age as the magnetization age.

4.5. Antigua

4.5.1. Paleomagnetic Interpretations

The NRM of the lava and the granodiorite of the Basal Volcanic Suite ranges from 50 to 1,500 mA/m. A soft north-pointing component recognized in the range of 0–20 mT or room temperature to 300°C, is interpreted as a present-day field overprint (Figure 5m). Sampling location AND1 and NH2 yielded strongly scattered directions

that we did not include in further analysis. Gyroremance is suspected for the sampling locations DAC, NH1, and BE at high coercivity steps beyond ~80 mT as remaining magnetization directions after AF treatments are going away radially from the mean direction (Figure 5o). We interpreted the component decaying toward the origin at the lower-coercivity steps in those cases. The reverse polarity granodiorite sampling location (GR) contains a north-directed normal overprint. AF demagnetized samples simultaneously unblock the ChRM and this overprint component leading to great circle trajectories (Figure 5p). The NRM of the tuffs (TU1, TU2) ranges from 16 to 380 mA/m. The NRM of the siltstone (CO, FJ) and lacustrine limestones (CH1 to 5, FI) sampling locations range respectively from 0.1 to 126 mA/m and from 0.1 to 2300 mA/m. The large intensity range of the lacustrine limestones is explained by variations of their detrital content and possibly lighting strike overprints (see sampling location CH5). A north-directed, normal overprint is observed at low-coercivity and low-T steps (viscous component, Figure 5l). Reverse and normal components form stable magnetic components in many samples, in the range of 20–120 mT or 400° to 600°C. KT experiments indicate that MD (with minor SD grains) magnetite and titano-magnetite are the main magnetic carriers (Figure S1 in Supporting Information S1). Nevertheless, the KT experiment also outlines the presence of secondary phases (probably pyrrhotite), recognized in both magmatic and volcano-sedimentary specimens. The sulfides most probably originated from an hydrothermal event that potentially partly or totally overprinted the primary magnetization. We interpreted a ChRM component for the Antigua specimen only for the temperature superior to the blocking temperature of pyrrothite (~320–350°C). We also interpret a ChRM component for the AF diagrams that were demagnetizing correctly as pyrrhotite is not supposed to demagnetize in AF (Figure 5m). At sampling locations TU1 and CO, we recognized two antipodal components on both AF and THe magnetization diagrams. The first is normal and observed from 0 to 20 mT or 25–300°C. The second is normal or reverse and observed from 60 to 120 mT or 480–600°C (Figure 5n). We interpreted this latter as the ChRM. Low NRM, ranging between 0.01 and 3.2 mA/m, characterizes the limestones of the Antigua Formation. Normal and reversed components are interpreted in the range of 10–80 mT or 200–450°C. Samples from PB sampling location yielded relatively stable demagnetization diagrams, but the directions are dispersed and not consistent with the data set. These outlier specimens have a high intensity NRM (up to 130 mA/m) and a reddish color. In the other sampling locations, it is challenging to decipher between a ChRM and a secondary overprint as the demagnetization diagrams are noisy due to the low magnetization of the specimen and due to the potential presence of pyrrhotite. For the limestones, the KT experiments were not conclusive. Consequently, we do not use the directions from these sampling locations.

4.5.2. Data Collections

We compiled the mean direction of the lava sampling locations with the direction of the granodiorite and of the volcaniclastic specimens as they have a similar stratigraphic age (late Eocene to early Oligocene, Montheil et al., 2023) and show consistent directions (Table 1 and Figures 6 and 7). A positive reversal test was performed on this combined collection (Figure S3E in Supporting Information S1). The collection passes the Deenen et al. (2011) criterion. The ages of the Antigua units range from late Eocene to late early Oligocene (Montheil et al., 2023). Nevertheless, the magnetization age might be younger than the stratigraphic ages as the whole volcanic and sedimentary pile suffered a mid-Miocene thermal event that could have partially or totally remagnetized the samples. Due to the age uncertainty of the magnetization components, the Antigua data set is not used in later relative rotation estimates.

4.6. Martinique

4.6.1. Paleomagnetic Interpretations

The NRM of the Oligocene and Miocene lavas of Martinique ranges from 70 to 800 mA/m. AF and TH demagnetization diagrams show stable components. A normal, north-directed component is recognized at low temperature and low coercivity at some sampling locations and interpreted as a present-day field overprint (Figure 4j). Sampling locations have normal or reverse polarity and components in the range of 20–120 mT or 300–600°C are interpreted as the ChRM (Figure 5j). For most sampling locations, the interpreted direction is well clustered ($k > 100$, Table 1) indicating measuring errors are small. The range of AF and TH demagnetization and KT experiments indicates that titano-magnetite is the main magnetic carrier and that some specimens contain minor sulfurs (Figure S1 in Supporting Information S1). Sampling locations FM1, FM2, TM show an outlier component, not demagnetizing at high-coercivity and demagnetizing at high-T steps, likely carried by secondary goethite, whose presence is suspected by KT experiment (Figure S1 in Supporting Information S1). A high intensity component

with NRM comprised between 100 and 3,044 mA/m quickly demagnetized with AF treatment of maximum 20 mT is observed at sampling locations BM, BR, CC, CL, LEN, MA, OL PV1, PV2, PV3, SK, SZ, TA, TP, and TT (Figure 5k). The demagnetization diagrams of these sampling locations show noisy trends and some specimens have great circle trajectories (Figure 5k) and outlier directions. We attribute this component to lightning overprints. Overall, the ChRM remains visible at high demagnetizing and high temperature steps (Figure 5k). The limestones, sampled at sampling locations GM and MBF, yielded no meaningful result due to a very low magnetization (NRM: 0.005–0.05 mA/m).

4.6.2. Data Collections

We compiled the mean directions of Martinique samples in two collection, one for the Oligocene lavas of the Sainte-Anne and la Caravelle Fm. and one for the Miocene lavas of the Vauclin Pitault Fm (Table 1 and Figures 6 and 7). A positive reversal test was performed for these two collections indicating similar ChRM direction of the Oligocene and Miocene lavas (Figure S3F in Supporting Information S1). Both collections pass the Deenen et al. (2011) criterion. We performed a conglomerate test on a Miocene conglomerate located within the Vauclin Fm. (sampling location NZ, Figure S4 in Supporting Information S1). The interpreted ChRM directions are dispersed and do not show any consistency ($K = 1.3$) indicating that the sampled blocks were magnetized before deposition. Owing to the positive conglomerate and reversal tests and stable demagnetization diagrams, we interpret the directions from the lava flows of Vauclin-Pitault Fm, Sainte-Anne Fm and la Caravelle Fm as primary, middle to late Miocene, and late Oligocene magnetizations, respectively.

5. Constraining Relative Tectonic Rotations

5.1. Approach

Paleomagnetism is a powerful tool to quantify relative displacements of tectonic terranes back in geological time (e.g., Coe et al., 1985; Demarest, 1983). The conventional approach to determine such displacements is to first compute a "grand" mean paleomagnetic direction or its associated paleomagnetic pole by averaging a collection of paleomagnetic directions or VGPs obtained from different paleomagnetic sites (each interpreted as a spot reading of the past geomagnetic field). This direction or pole is then compared with a reference direction or pole predicted by a (global) apparent polar wander path (APWP) (e.g., Torsvik et al., 2012), providing an estimate of the rotation or paleolatitudinal displacement of the studied terrane relative to the chosen reference plate. The uncertainty is typically calculated as the square root of the sum of the squared 95% confidence limits uncertainties, for example, corresponding to the A_{95}, ΔD or ΔI values (Butler, 1992; Demarest, 1983).

However, Rowley (2019) recently showed that when using this approach more than half of the input paleomagnetic poles of the global APWP by Torsvik et al. (2012) are statistically different from the APWP itself. This suggests that the conventional comparison method of an individual paleomagnetic data set with a reference APWP may not provide a robust estimate of relative tectonic displacements, such as vertical-axis rotations. Vaes et al. (2022) proposed an alternative VGP-based comparison approach in which two paleomagnetic data sets are compared at the level of VGPs instead of a comparison between paleomagnetic poles. In this approach, the studied paleomagnetic data set is compared to a reference pole that is defined by the same number of VGPs that are included in the studied data set. For instance, a paleomagnetic data set of 18 sites would be compared with a set of random draws (or re-sampling) of the 18 VGPs from the reference data set (see Vaes et al. (2022) for more details).

Here, we build upon the approach of Vaes et al. (2022) and use an equal-N comparison method to determine relative tectonic rotations in the Caribbean region (Figure 8). This method iteratively compares the difference in declination between two collections of paleomagnetic data, whereby the confidence bounds of the largest data collection is recalculated and weighted against the number of directions of the smallest collection. For each bootstrap iteration, the paleomagnetic directions of the studied block (with the lowest number of sites) are first re-sampled with replacement. Next, a reference paleomagnetic direction is computed from a paleomagnetic pole that is calculated as the mean of a random draw (with replacement) of the same number of VGPs as the number of directions obtained for the studied block. We then follow an approach similar to that of Calvagno et al. (2020) to compute the relative rotation and its confidence limits. We compute the difference in declination between each re-sampled direction and the reference paleomagnetic direction and subsequently average those differences to obtain a single estimate of the relative rotation ΔR_i (for the ith iteration). Finally, the relative tectonic rotation

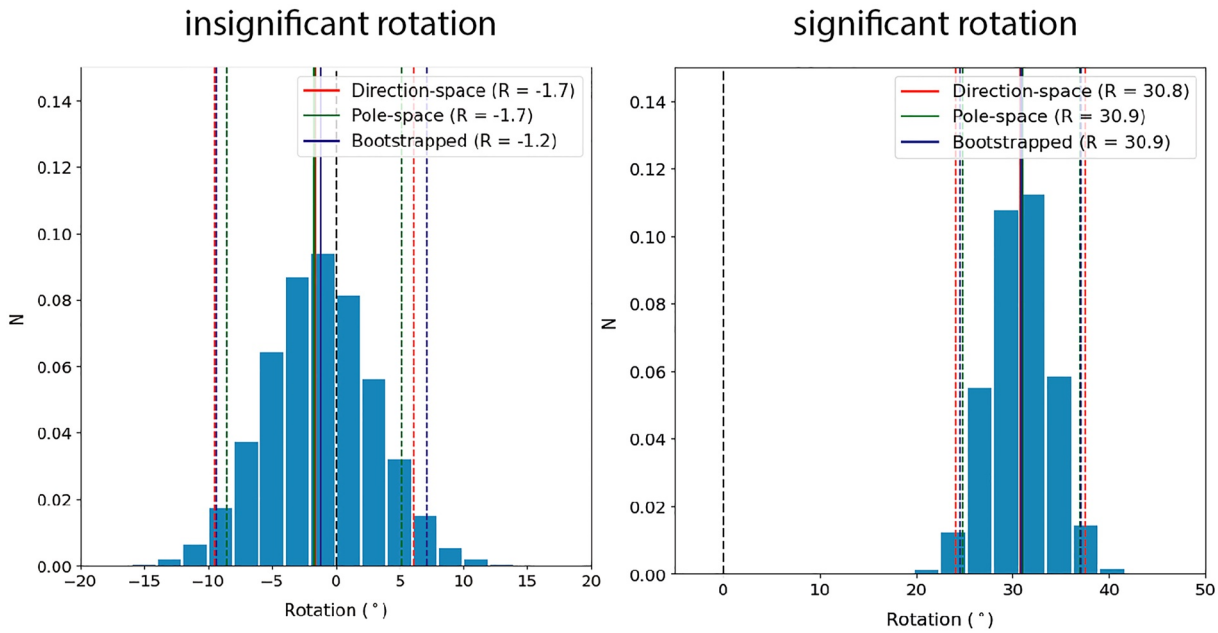

Figure 8. Example of differential paleorotation estimate between two collections using the classical pole-space (in green), direction space approach (in red) of Butler (1992) and the bootstrapped approach used in this study (in blue). The 95% confidence ellipse values are represented by the dotted lines. The rotation is statistically significant when the confidence ellipses do not overlap 0° of rotation (black dotted line). (a) Example of a not significant differential paleo-rotation, from Puerto Rico upper Oligocene collection compared to the Puerto Rico lower Miocene collection; (b) Example of significant differential paleorotation, from Saint-Martin lower Oligocene collection compared to the Saint-Martin-Anguilla upper Miocene collection.

is quantified by the mean of 10,000 ΔR values, and its 95% confidence limits are defined by the range in which 95% of the rotation estimates fall (Figure 8). As shown in the example in Figure 8, the rotational values are nearly identical to that using the conventional approach (both in direction- or pole-space, see Butler, 1992). However, the confidence regions tend to be more conservative, particularly when the studied data set has relatively small N (see also Vaes et al., 2022). We note that the bootstrapped confidence limits become similar to those of the conventional approach in cases where the number of sites in the collections of the studied and reference blocks is similar.

We apply this approach to establish whether there are rotational differences between our collections and previous collections from the NE Caribbean region. We included the previous paleomagnetic collections in our data table, and parametrically resampled these collections to conduct the paleomagnetic analysis following the methods described above. We first compare the relative rotation between collections from islands of the same tectonic block. If there is no relative rotation between collections of the same age range, they are combined into a larger collection. We then compare the collections of the same block with different ages, from the older collection to the next youngest one, to quantify the cumulative rotation as a function of time. Finally, we compare the collection of different blocks of the same age to check on the relative rotation between tectonic blocks. The relative rotation values are presented in Supplementary Information 5. To compare rotations of the northeastern Caribbean blocks to a stable plate such as North America or the Caribbean plates, a global APWP should be computed based on sampling location-level data rather than paleopoles (Vaes et al., 2022). Such a path is currently unavailable. We therefore illustrate the trends in rotation in the northeastern Caribbean from our study against the global APWP of Torsvik et al. (2012) in the coordinates of North America, as well as in the coordinates of the Caribbean plate interior determined from the reconstruction of Boschman et al. (2014) (Figures 7 and 9). We note that Boschman et al. (2014) reconstructed the Caribbean plate motion relative to North America using the Cayman Trough spreading records of Leroy et al. (2000), assuming that the Caribbean plate interior formed the conjugate to the North American plate in that spreading system. However, this reconstruction ignored the motion along the Enriquillo-Plantain Garden fault zone, which separates the Gonave microplate from the Caribbean plate interior. If future, more detailed kinematic reconstructions need to modify the Caribbean-Gonave microplate rotation, this will affect the predicted APWP in Caribbean plate coordinates. With these caveats in mind, we are careful to not over-interpret the quantitative differences, but we evaluate whether trends in rotation are similar, or not, to those

Figure 9. Diagram of the relative rotations and relative uncertainties compared to the geographic north plotted against the ages of the collection. The color of the collections follows the same code as in Figure 7. Rotation trends of the studied blocks are outlined by the thick dotted lines and interpreted according to relative rotation estimates.

of the neighboring plates and only indicate a rotation compared to the north geographic pole as an indicative value that will need to be re-evaluated with an updated Caribbean plate motion reconstruction (Figure 9).

5.2. Relative Rotation per Block

5.2.1. Puerto Rico—Virgin Island Block

There is no significant difference between the VGP computed from the Bath pluton, the Salt pluton, and the Necker Formation collections (Figure 9 and Table S1). This indicates that no statistically significant rotations are demonstrated within each pluton, or between the upper Eocene (Bath pluton) and the lower Oligocene (Salt pluton) of the British Virgin Islands. Compared to the Necker Tuffs and the Bath pluton collections, the middle Eocene Virgin Gorda pluton, a just-significant counterclockwise (CCW) rotation of 18° ± 14° and 17° ± 15° respectively (Table 1). Compared to the north pole, the Bath and Salt Pluton, have a relative rotation of ∼45° ± 8° (Figure 9). The BVI collections are statistically significant relative rotation with the late Cretaceous to Eocene VGP of van Fossen et al. (1989) (Figure 9 and Table S1). The lower upper Oligocene collection of Puerto Rico does not show significant rotation compared to the lower Oligocene collection of BVI (Salt pluton). Relative to the Salt and the lower upper Oligocene collections, the upper Oligocene collection of Puerto Rico reveals a differential CCW rotation of 25° ± 7° and 17° ± 10° respectively. Compared to the geographic north, the upper Oligocene collection has a relative rotation of ∼19° ± 7°. The lower Miocene collection of Puerto Rico does not show statistically significant rotation with the upper Oligocene collection. Relative to the middle to upper Miocene and Pliocene collection that have a similar mean direction, the lower Miocene collection has a relative rotation of 15° ± 11°. The mid-upper Miocene and Pliocene collection of Puerto Rico are comparable to the geographic north indicating a stop in the rotation of the PRVI block by the middle Miocene (Figure 9 and Table S1).

Collectively, these data constrain a 45° ± 8° counterclockwise rotation of the Puerto Rico-Virgin Island Block since the middle Eocene. The single sampling location of the small Virgin Gorda collection may suggest that rotations also occurred between the early and middle Eocene, but our collection is not large enough to firmly establish the amount or regional extent of this rotation. This rotation is consistent with the values presented by van Fossen et al. (1989) who estimated a post-Eocene CCW rotation of ∼45° compared to North America. The relative rotation estimates, and the rotation trend presented in Figure 9, outline a rapid rotation (∼5°/Myr, Figure 9) of the PRVI block, of up to 25° ± 7° during the Oligocene followed by a rotation of 15° ± 11° since the early Miocene and a cessation of the rotation during the middle Miocene. The timing of this cessation is much older than the previous estimation of Reid et al. (1991) who proposed a cessation in Pliocene after a CCW rotation of 22° between 11 and 4.5 Ma. We explain this difference by using a small middle Miocene data set in this previous study that might have led to an overestimation of the middle Miocene rotation. Our refined counterclockwise rotation history is considerably larger than that predicted by the Global Apparent Polar Wander Path of Torsvik et al. (2012), rotated in North American and Caribbean coordinates, which show counterclockwise rotations of not more than ∼10° (Figures 7 and 9) in Oligocene to Miocene time.

5.2.2. Northern Lesser Antilles Block

Compared to the Oligocene collection of Saint-Martin, which comprises combined directions and associated poles interpreted from lavas and granodiorite specimens, the middle to upper Oligocene collection of Saint-Barthélemy reveals a statistically significant CCW rotation of 10° ± 7°. Relative to the geographic North, these collections indicate a CCW rotation of 38° ± 6° and 24° ± 4° respectively (Figure 9 and Table S1). Both lower to middle Miocene and upper Miocene Saint-Martin and Anguilla collections were combined as they have the same biostratigraphic age (Cornée et al., 2021), and as the collections from the two islands do not reveal significant relative rotation (Figure 9 and Table S1). Relative to the Saint-Barthélemy collection, the combined Saint-Martin-Anguilla lower to middle Miocene collection does not show statistically meaningful rotation. Compared to the Saint-Martin-Anguilla lower to middle Miocene collection, the Saint-Martin-Anguilla upper Miocene collection reveals a relative rotation of 18° ± 9° (Figure 9 and Table S1). The Antigua collection was not used for relative rotation due to the uncertainty of its magnetization age (i.e., either late Eocene—early Oligocene if primary, or mid-Miocene if remagnetized).

Collectively, these data reveal a 38° ± 6° CCW rotation of the Northern Lesser Antilles block since the early Oligocene compared to the geographic north. The rotation trend and relative rotation estimate indicates a rapid CCW rotation (~5°/Myr, Figure 9) of 20° ± 7° during the Oligocene followed by a CCW rotation of 18° ± 9° during the Miocene and a cessation of the rotation by the late Miocene. This rotation history is larger than the Oligocene to Miocene rotation predicted by the Global Apparent Polar Wander Path of Torsvik et al. (2012) rotated in North American and Caribbean coordinates (Figures 7 and 9).

5.2.3. Martinique

We compared the Oligocene collection of Martinique to the Miocene collections of the same island and observed no statistically significant rotation (Figure 9 and Table S1). Compared to the middle Eocene collection of Speed et al. (1997), estimated from 15 basalt sampling locations, the Oligocene collection of Martinique does not show significant rotation. These collections have a declination comparable to the declination trend of the APWAP of Torsvik et al. (2012) rotated in North American and Caribbean coordinates and to the geographic north (Figures 7 and 9) suggesting that Martinique and the Grenadines did not rotate since the upper Oligocene.

5.3. Relative Rotation Between Blocks

In this section we compare collections of the same age of the PRVI, NoLA, and SoLA blocks. We find that there is no significant declination difference between the lowermost Oligocene collection of Puerto Rico to the lower Oligocene collection of Saint-Martin, nor between the upper lower Oligocene collection of Puerto Rico to the middle-upper Oligocene of Saint-Barthélemy (Figure 9 and Table S1). This indicates that the PRVI and NoLA blocks did not demonstrably rotate relative to each other between the latest Eocene and late Oligocene (Figure 9), which is in line with the conclusion that during the Paleogene, the faults of the Anegada Passage did not exist yet (Cornée et al., 2021; Laurencin et al., 2017).

We then compare the lower Miocene collection of Puerto Rico with the Saint-Martin-Anguilla lower to middle Miocene and the middle to upper Miocene collection of Puerto Rico to the upper Miocene collection of Saint-Martin-Anguilla. The total amount of estimated Miocene rotation that the two blocks underwent is equal (~20°), the timing of cessation of rotation is earlier (middle Miocene) for the PRVI block, compared to the one of the NoLA block (late Miocene) (Figure 9).

Relative to the middle Eocene collection of Grenadines (Speed et al., 1997), the middle Eocene Virgin Gorda and the upper Eocene Bath pluton collection reveal a CCW rotation of 60° ± 13° and 45° ± 15° respectively. The comparison between the middle-upper Oligocene collection of Saint-Barthélemy with the upper Oligocene collection of Martinique indicates a just-significant counterclockwise rotation of 15° ± 14°. Between the middle to upper Miocene collection of Martinique and the upper Miocene collection of Saint-Martin-Anguilla, no significant rotation is observed. From the Eocene to Oligocene, the rotational trend of Martinique and the Grenadines islands is comparable to the Caribbean and North American one and clearly differs from the PRVI and NoLA ones (Figure 9). During the Miocene, these rotational trends merged as the PRVI and NoLA blocks stopped their rotation. Although the data set for the SoLA Block is much smaller than for NoLA, the available data suggest that the SoLA Block did not partake in the counterclockwise rotation episode, and that a structure accommodating the rotation difference is to be sought north of Martinique (Figure 9).

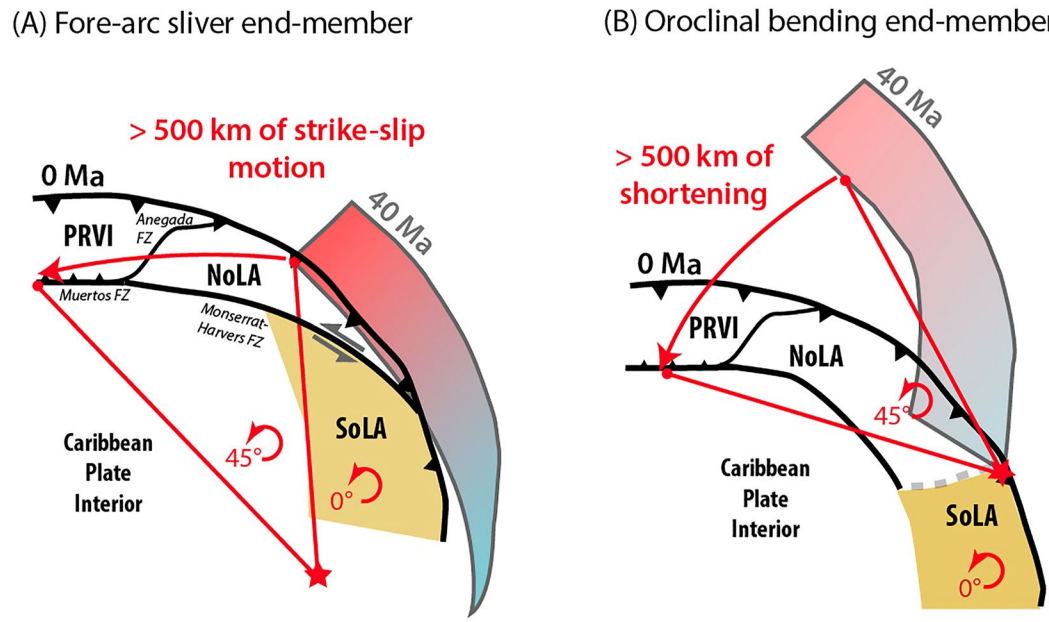

Figure 10. Schematic representation of the NE Caribbean intraplate deformation end-member mechanisms. The rotation poles relative to the Caribbean Plate interior are represented by the purple stars. The sense and amount of rotation are represented in red.

6. Tectonic Implications of Block Rotations

Our new paleomagnetic analysis reveals that much larger rotations occurred in the NE Caribbean region than hitherto accommodated in kinematic reconstructions (e.g., Boschman et al., 2014; Montes et al., 2019; Pindell & Kennan, 2009). The net rotation difference between the PRVI and NoLA blocks is zero, but during the Miocene, the PRVI block rotated more rapidly than the NoLA block (Figure 9). By that time, the Anegada passage, a major transtensive fault zone whose activity is likely linked to the exhumation of the granodioritic plutons and metamorphic rocks of the Virgin Islands (Roman et al., 2021) started to be active (Cornée et al., 2021; Laurencin et al., 2017). We postulate that the initiation of this fault zone tectonically separated the PRVI and NoLA block and accommodated part of the differential Miocene rotation rate between the PRVI and NoLA block by strike-slip motion.

The rotation difference between the SoLA block that did not undergo rotation, and the PRVI and NoLA blocks, that underwent 45° of CCW rotation or more since the late Eocene, requires larger motion along faults zones than hitherto thought. To explore the first-order implications, we discuss three end-member scenarios.

On the one hand, rotation may be explained by the motion of a forearc sliver that includes the NoLA and PRVI block along the northeastern corner of the Caribbean plate, partitioning Caribbean-North America plate motion. In this scenario, the forearc sliver motion is accommodated by sinistral strike-slip along a major fault located at the back of the PRVI and NoLA block. The candidate fault zones are the curving NW-SE Monserrat-Harvers fault zone connecting to the E-W trending structure that later becomes the Muertos Trough (Figure 10a). Such a scenario implies a polyphased history of the Muertos Trough with strike-slip motion preceding more recent transpression and/or shortening. This has already been proposed by Pindell and Kennan (2009) in their reconstruction but has not yet been confirmed by direct observations (Granja-Bruna et al., 2010). To accommodate the required 45° CCW rotation, we estimate a westward sliver displacement on the order of ∼500 km (Figure 10a). This scenario is quite similar to the one proposed by Gomez et al. (2018). These authors estimated a ∼350 km left-lateral displacement along a southern extension of the Monserrat-Harvers fault to replace the Mesozoic stratigraphic units of la Desirade Island in front of similar units recognized in the Barbados-Tobago ridge. The forearc sliver scenario displaces the NoLA block on the order of 500 km farther to the south-east, right to the east of the SoLA block, back to the late Eocene (Figure 10a). This position is consistent with the magmatic record of the Lesser Antilles arc and may help resolve the quest of the ancient magmatic arc in the southern

Lesser Antilles (Aitken et al., 2011; Allen et al., 2019; Garrocq et al., 2021). Indeed, Paleogene magmatic rocks are only exposed at both extremities of the Lesser Antilles arc, that is, in the Northern Lesser Antilles and to the south east of the Lesser Antilles Arc maybe in Grenada Island and between Los Testigos and Margarita islands (Aitken et al., 2011; Allen et al., 2019; Montheil et al., 2023). In this scenario, the Grenada basin would have been located in a back-arc position during that time (Figure 10a). It is also important to note that the PRVI block was connected to the Hispaniola Block and the Gonave microplate since the Eocene, whose motion relative to the Cuban segment (i.e., part of North America since the late Eocene, Iturralde-Vinent et al., 2008) is determined by the Cayman Trough ocean floor spreading. None of these relationships change due to the rotation which is consistent with the absence of E-W compression between the PRVI and Hispaniola block, which are separated by the Oligocene Mona rift (Mondziel et al., 2010). The forearc sliver scenario thus requires that the eastward motion of the Caribbean Plate interior relative to North America was on the order of ∼500 km more than the spreading accommodated in the Cayman Trench.

The second end-member scenario is oroclinal bending of the Lesser Antilles and the Puerto Rico trenches about a pole that coincides with the boundary between NoLA and SoLA (Figure 10b). In this scenario, the 45° of CCW rotation would require a westward increasing shortening up to ∼500 km at the back of the PRVI and NoLA blocks, between these blocks and the Caribbean plate interior and about 100 km of extension between the NoLA and SoLA blocks (Figure 10b). That shortening occurrence is evident from the Muertos Trough, which is located south of Puerto Rico (Granja-Bruna et al., 2010; Laó-Dávila, 2014) but not in the Monserrat-Harvers fault zone, where only transtension and normal faulting have been evidenced (Feuillet et al., 2011). Imaging of the Muertos Trough structure recognized that the Muertos thrust does not extend farther than 150 km north of the deformation front (Byrne et al., 1985; Granja-Bruna et al., 2010; van Benthem et al., 2013), which should be considered as a maximum displacement. Shortening that could have accommodated this type of rotation was evidenced recently within the NoLA block (Philippon, Cornée, et al., 2020). However, this shortening occurred in middle Eocene time, that is, prior to the NoLA rotation documented here, and there is no evidence for younger shortening there. So, we conclude that while the shortening accommodated by the Muertos Trough may have accommodated some of the rotation documented in this paper, the oroclinal bending endmember likely only had a subordinate contribution to the net rotation of the PRVI and NoLA blocks and that the fore-arc sliver scenario is probably the dominant mechanism of rotation accommodation.

In these two scenarios, the PRVI and NoLA blocks behave as a large monolithic and coherent rotating block. Structural studies in Puerto Rico (Mann et al., 2005; Lao-Davila et al., 2014) and in the Northern Lesser Antilles back-arc (Philippon, Cornée, et al., 2020) and fore-arc (Boucard et al., 2021) have shown that these blocks display evidence of crustal deformation that could have potentially contributed to rotation differences. We may thus explore the possibility that the rotations are accommodated by smaller tectonic blocks in a bookshelf style. Such a scenario was initially proposed by MacDonald (1980) to account for the CCW rotation of the Greater Antilles blocks. Such a scenario still requires the presence of two major bounding fault zones between which the fault-bounded blocks rotate, one of which is the Lesser Antilles-Puerto Rico Trench, and for the other the Montserrat-Harvers Fault connecting to the Muertos Trough is again the best candidate. The faults bounding the counterclockwise rotating blocks must then be dextral strike-slip faults with either a compressional or a transtensional component. In the NE Caribbean region, the only candidate fault for such a mechanism is the Anegada Passage (Figures 1 and 10). The V-shape faults of the Lesser Antilles fore-arc also likely accommodate some rotation difference, but only in the outer forearc (Boucard et al., 2021), and cannot explain the rotations farther inboard of the Caribbean Plate. Only the Anegada Passage is insufficient to accommodate bookshelf-style block rotations and there are no other cross-block faults known from the NE Caribbean so we consider this scenario unlikely. And even if it were the case, this would be a mere variation on the forearc sliver scenario. We thus consider the monolithic block models the most likely scenario, with some combination of oroclinal bending and fore-arc sliver motion, with this latter being the dominant mechanism. Incorporation into detailed kinematic reconstructions of the Caribbean region may reveal the relative contributions of these two components to the NE Caribbean tectonic history.

7. Paleogeographic Implications

The fore-arc sliver scenario would restore the PRVI and NoLA block about 500 km to the southeast back to the Eocene, allowing a potential connection with the South American continent (Figure 10a). Within these blocks,

middle Eocene to early Oligocene regional unconformities and erosional surfaces indicate the presence of a large emergent area (Cornée et al., 2020, 2021). During that time, intense magmatic activity developed in the Northern Lesser Antilles block, leading to the emergence of volcanic edifices (Montheil et al., 2023). Moreover, the late Eocene compressive tectonics evidenced in the PRVI and NoLA blocks may have contributed to the thickening and regional emersion of these blocks (Lao-Davila et al., 2014; Philippon, Cornée, et al., 2020; GraNoLA land). The potential southeastern position of the Northern Lesser Antilles block and the presence of middle Eocene to early Oligocene emergent land thus define the Northern Lesser Antilles as a potential pathway for South American fauna dispersals. This represents an alternative or complementary solution to the GAARlandia hypothesis that considered the Aves ridge as the only potential pathway for South-American faunas (Iturralde-Vinent & MacPhee, 1999). This scenario is not contradictory to the GAARlandia hypothesis but indicates that the PRVI and NoLA blocks may have played a prominent role in terrestrial fauna dispersal during the Cenozoic. Our results thus open new conceptual possibilities to explain the enigmatic paleobiogeography of the Caribbean region, but evaluating the full breath of the opportunities provided by our new paleomagnetic data requires a detailed, Caribbean-wide re-evaluation of the Cretaceous-Cenozoic kinematic and paleogeographic history.

8. Conclusion

In this study, we show a large paleomagnetic data set from the deformed corridor of the northeastern Caribbean Plate, including novel data from Puerto Rico, the British Virgin Islands, Anguilla, St. Martin, Antigua, and Martinique. We use a statistical bootstrap approach to quantify the relative rotation histories of three, mostly submerged crustal blocks of the northeastern Caribbean: the Puerto Rico-Virgin Island Block, and the Northern and Southern Lesser Antilles Blocks. We show that.

1. The Puerto Rico-Virgin Island block underwent counterclockwise (CCW) rotation of 45 ± 8° relative to the geographic north since middle to late Eocene decomposed in 25° ± 7° CCW rotation during the Oligocene and 15° ± 11° CCW rotation during the early Miocene and that this rotation stopped by the middle Miocene.
2. The Northern Lesser Antilles block underwent a 38° ± 6° CCW rotation relative to the geographic north since the early Oligocene decomposed in 20° ± 7° CCW rotation during the late Oligocene and 18° ± 9° CCW rotation during the early and middle Miocene and that this rotation stopped by the late Miocene.
3. The Puerto Rico-Virgin Island and Northern Lesser Antilles block formed a coherent monolithic rotating block until the late Oligocene but became two independently rotating blocks during the early Miocene with the opening of the Anegada passage that likely accommodated part of the block rotations.
4. The Southern Lesser Antilles was forming an independent non-rotating block from the Eocene to the middle-late Miocene, probably bounded to the north by the Monserrat-Harvers fault zone.
5. The counterclockwise rotations of the Puerto Rico—Virgin Islands and Northern Lesser Antilles blocks are much larger than previously thought in kinematic reconstructions and we discuss end-member solutions to accommodate these rotations. On the one hand, the northeastern Caribbean block rotations may have been part of a forearc sliver that moved around the curved plate boundary. This end-member requires motions relative to the Caribbean Plate interior on the order of 500 km. On the other hand, oroclinal bending of the trench could accommodate the rotations, requiring on the order of 500 km of intra-plate shortening at the longitude of the Muertos Trough. The latter option may have contributed but is unlikely to be the sole solution to the rotation problem.

This intraplate deformation invites revisiting the detailed kinematic reconstruction of the Caribbean region, which is beyond the scope of this paper. Nonetheless, we foresee that this updated reconstruction will have major implications for the paleogeography of the eastern Caribbean region. Large-scale forearc sliver motion would restore the emerged Paleogene lands reconstructed in the northeastern Caribbean (GRANoLA) much farther to the south than previously thought, forming with GAArlandia an interesting avenue to explore the enigmatic land fauna dispersal between South America and the Lesser and Greater Antilles in the Paleogene.

Data Availability Statement

Data: The data used for the paleomagentic analysis are presented as .col files. These files contain the directions for each sample at each demagnetizing step. The directions are represented with Zijderveld and intensity diagrams and with stereographic projections. These diagrams are accessible in uploading the .col files in paleomagnetism.org.

The data are in open access and accessible in the Zenodo repository at https://doi.org/10.5281/zenodo.7791447 (Montheil, 2023). *Software*: The paleomagnetic data analysis was underwent with the open source online software paleomagnetism.org (Koymans et al., 2016, 2020) accessible at: https://paleomagnetism.org.

Acknowledgments
The authors would like to warmly thank Patrick Nicol of the University of Montpellier for his help in the Paleomagnetic Laboratory as well as Maxime Kasparov and Mark Dekkers of the University of Utrecht for their assistance in the Fort Hoofddijk Paleomagnetic Laboratory. A special thank goes to Chris Waters and Dr. Reg Murphy of the National Park of Antigua and to the National Park of La Caravelle in Martinique for allowing access to special sites, and to Olivia Urity and Victoria Boirard for their help in the field in Martinique and Antigua. We warmly thank James Joyce and Tom Hudgins for bringing us for an introductory fieldwork in the BVI during spring break 2019 and for their precious advices they gave during the preparation of the 2021 sampling campaign of the BVI. This work was supported by the GAARAnti project (ANR-17-CE31-0009) and by the INSU TelluS-SYSTER Grant call for 2017–2019. D.J.J. van Hinsbergen acknowledges Netherlands Organization for Scientific Research (NWO) Vici Grant 865.17.001. We thank Paul Mann and an anonymous reviewer for constructive reviews.

References

Aitken, T., Mann, P., Escalona, A., & Christeson, G. L. (2011). Evolution of the Grenada and Tobago basins and implications for arc migration. *Marine and Petroleum Geology*, *28*(1), 235–258. https://doi.org/10.1016/j.marpetgeo.2009.10.003

Allen, R. W., Collier, J. S., Stewart, A. G., Henstock, T., Goes, S., & Rietbrock, A. (2019). The role of arc migration in the development of the Lesser Antilles: A new tectonic model for the Cenozoic evolution of the eastern Caribbean. *Geology*, *47*(9), 891–895. https://doi.org/10.1130/g46708.1

Andreieff, P., Baubron, J. C., & Westercamp, D. (1988). Histoire Géologique de la Martinique (Petites Antilles): Biostratigraphie (foraminifères), radiochronologie (potassium–argon), évolution volcano-structurale. *Géologie de la France*, *2*(3), 39–70.

Benford, B., DeMets, C., & Calais, E. (2012). GPS estimates of microplate motions, northern Caribbean: Evidence for a Hispaniola microplate and implications for earthquake hazard. *Geophysical Journal International*, *191*(2), 481–490. https://doi.org/10.1111/j.1365-246x.2012.05662.x

Benford, B., Tikoff, B., & DeMets, C. (2012). Character of the Caribbean–Gônave–North America plate boundaries in the upper mantle based on shear-wave splitting. *Geophysical Research Letters*, *39*(24). https://doi.org/10.1029/2012GL053766

Boschman, L. M., van Hinsbergen, D. J., Torsvik, T. H., Spakman, W., & Pindell, J. L. (2014). Kinematic reconstruction of the Caribbean region since the early Jurassic. *Earth-Science Reviews*, *138*, 102–136. https://doi.org/10.1016/j.earscirev.2014.08.007

Boucard, M., Marcaillou, B., Lebrun, J. F., Laurencin, M., Klingelhoefer, F., Laigle, M., et al. (2021). Paleogene V-shaped basins and Neogene subsidence of the Northern Lesser Antilles forearc. *Tectonics*, *40*(3), e2020TC006524. https://doi.org/10.1029/2020TC006524

Bouysse, P., Garcia-Reyes, A., de Lépinay, B. M., Ellouz-Zimmermann, N., & Pubellier, M. (2020). Structural map of the Caribbean, scale 1: 4M.

Burke, K. (1988). Tectonic evolution of the Caribbean. *Annual Review of Earth and Planetary Sciences*, *16*(1), 201–230. https://doi.org/10.1146/annurev.ea.16.050188.001221

Butler, R. F. (1992). *Paleomagnetism: Magnetic domains to geologic terranes* (Vol. 319). Blackwell Scientific Publications.

Byrne, D. B., Suarez, G., & McCann, W. R. (1985). Muertos Trough subduction—Microplate tectonics in the northern Caribbean? *Nature*, *317*(6036), 420–421. https://doi.org/10.1038/317420a0

Calais, E., Camelbeeck, T., Stein, S., Liu, M., & Craig, T. J. (2016). A new paradigm for large earthquakes in stable continental plate interiors. *Geophysical Research Letters*, *43*(20), 10–621. https://doi.org/10.1002/2016GL070815

Calais, E., Symithe, S. J., & de Lépinay, B. M. (2023). Strain partitioning within the Caribbean–North America transform plate boundary in southern Haiti, tectonic and hazard implications. *Bulletin of the Seismological Society of America*, *113*(1), 131–142. https://doi.org/10.1785/0120220121

Calcagno, P., Bouchot, V., Thinon, I., & Bourgine, B. (2012). A new 3D fault model of the Bouillante geothermal province combining onshore and offshore structural knowledge (French West Indies). *Tectonophysics*, *526*, 185–195. https://doi.org/10.1016/j.tecto.2011.08.012

Calvagno, J. M., Gallo, L. C., Tomezzoli, R. N., Cristallini, E. O., Farjat, A. D., & Hernández, R. M. (2020). A new constraint on the central Andean rotation pattern from paleomagnetic studies in the southern Subandes of Bolivia. *Journal of South American Earth Sciences*, *98*, 102470. https://doi.org/10.1016/j.jsames.2019.102470

Carew, J. L., Mylroie, J. E., Vacher, H. L., & Quinn, T. M. (1997). Geology of the Bahamas. *Geology and hydrogeology of carbonate islands* (pp. 91–139).

Chaytor, J. D., & Ten Brink, U. S. (2010). Extension in Mona Passage, northeast Caribbean. *Tectonophysics*, *493*(1–2), 74–92. https://doi.org/10.1016/j.tecto.2010.07.002

Coe, R. S., Globerman, B. R., Plumley, P. W., & Thrupp, G. A. (1985). Paleomagnetic results from Alaska and their tectonic implications.

Corbeau, J., Rolandone, F., Leroy, S., De Lepinay, B. M., Meyer, B., Ellouz-Zimmermann, N., & Momplaisir, R. (2016). The northern Caribbean plate boundary in the Jamaica Passage: Structure and seismic stratigraphy. *Tectonophysics*, *675*, 209–226. https://doi.org/10.1016/j.tecto.2016.03.022

Cornée, J. J., Boudagher-Fadel, M., Philippon, M., Léticée, J. L., Legendre, L., Maincent, G., et al. (2020). Paleogene carbonate systems of Saint Barthélemy, Lesser Antilles: Stratigraphy and general organization. *Newsletters on Stratigraphy*, *53*(4), 461–478. https://doi.org/10.1127/nos/2020/0587

Cornée, J. J., De Min, L., Lebrun, J. F., Quillévéré, F., Melinte-Dobrinescu, M., BouDagher-Fadel, M., et al. (2023). Paleogeographic evolution and vertical motion of the central Lesser Antilles forearc since the early Miocene: A potential driver for land fauna dispersals between the Americas. *Marine and Petroleum Geology*, *152*, 106264. https://doi.org/10.1016/j.marpetgeo.2023.106264

Cornée, J. J., Münch, P., Philippon, M., Boudagher-Fadel, M., Quillévéré, F., Melinte-Dobrinescu, M., et al. (2021). Lost islands in the northern Lesser Antilles: Possible milestones in the Cenozoic dispersal of terrestrial organisms between South-America and the Greater Antilles. *Earth-Science Reviews*, *217*, 103617. https://doi.org/10.1016/j.earscirev.2021.103617

Cromwell, G., Johnson, C. L., Tauxe, L., Constable, C. G., & Jarboe, N. A. (2018). PSV10: A global data set for 0–10 Ma time-averaged field and paleosecular variation studies. *Geochemistry, Geophysics, Geosystems*, *19*(5), 1533–1558. https://doi.org/10.1002/2017GC007318

Dagain, J., Andréïeff, P., Westercamp, D., Bouysse, P., & Garrabe, F. (1989). *Notice et carte géologique de Saint-Martin 1/50 000, Antilles Françaises, Département de la Guadeloupe, éd* (Vol. 3). BRGM.

Deenen, M. H., Langereis, C. G., van Hinsbergen, D. J., & Biggin, A. J. (2011). Geomagnetic secular variation and the statistics of palaeomagnetic directions. *Geophysical Journal International*, *186*(2), 509–520. https://doi.org/10.1111/j.1365-246X.2011.05050.x

Demarest, H. H., Jr. (1983). Error analysis for the determination of tectonic rotation from paleomagnetic data. *Journal of Geophysical Research*, *88*(B5), 4321–4328. https://doi.org/10.1029/jb088ib05p04321

DeMets, C., Jansma, P. E., Mattioli, G. S., Dixon, T. H., Farina, F., Bilham, R., et al. (2000). GPS geodetic constraints on Caribbean-North America plate motion. *Geophysical Research Letters*, *27*(3), 437–440. https://doi.org/10.1029/1999gl005436

Feuillet, N., Beauducel, F., & Tapponnier, P. (2011). Tectonic context of moderate to large historical earthquakes in the Lesser Antilles and mechanical coupling with volcanoes. *Journal of Geophysical Research*, *116*(B10), B10308. https://doi.org/10.1029/1999GL005436

Feuillet, N., Leclerc, F., Tapponnier, P., Beauducel, F., Boudon, G., Le Friant, A., et al. (2010). Active faulting induced by slip partitioning in Montserrat and link with volcanic activity: New insights from the 2009 GWADASEIS marine cruise data. *Geophysical Research Letters*, *37*(19). https://doi.org/10.1029/2010gl042556

Fisher, R. A. (1953). Dispersion on a sphere. *Proceedings of the Royal Society of London, Series A: Mathematical and Physical Sciences*, *217*(1130), 295–305. https://doi.org/10.1098/rspa.1953.0064

Garrocq, C., Lallemand, S., Marcaillou, B., Lebrun, J. F., Padron, C., Klingelhoefer, F., et al. (2021). Genetic relations between the Aves Ridge and the Grenada back-arc basin, East Caribbean Sea. *Journal of Geophysical Research: Solid Earth*, *126*(2), e2020JB020466. https://doi.org/10.1029/2020jb020466

Germa, A., Quidelleur, X., Labanieh, S., Chauvel, C., & Lahitte, P. (2011). The volcanic evolution of Martinique Island: Insights from K–Ar dating into the Lesser Antilles arc migration since the Oligocene. *Journal of Volcanology and Geothermal Research*, *208*(3–4), 122–135. https://doi.org/10.1016/j.jvolgeores.2011.09.007

Gerritsen, D., Vaes, B., & van Hinsbergen, D. J. (2022). Influence of data filters on the position and precision of paleomagnetic poles: What is the optimal sampling strategy? *Geochemistry, Geophysics, Geosystems*, *23*(4), e2021GC010269. https://doi.org/10.1029/2021GC010269

Gomez, S., Bird, D., & Mann, P. (2018). Deep crustal structure and tectonic origin of the Tobago-Barbados ridge. *Interpretation*, *6*(2), T471–T484. https://doi.org/10.1190/INT-2016-0176.1

Granja-Bruña, J. G., Carbó-Gorosabel, A., Estrada, P. L., Muñoz-Martín, A., Ten Brink, U. S., Ballesteros, M. G., et al. (2014). Morphostructure at the junction between the Beata ridge and the Greater Antilles island arc (offshore Hispaniola southern slope). *Tectonophysics*, *618*, 138–163. https://doi.org/10.1016/j.tecto.2014.02.001

Granja Bruña, J. L., Muñoz-Martín, A., Ten Brink, U. S., Carbó-Gorosabel, A., Llanes Estrada, P., Martín-Dávila, J., et al. (2010). Gravity modeling of the Muertos Trough and tectonic implications (north-eastern Caribbean). *Marine Geophysical Researches*, *31*(4), 263–283. https://doi.org/10.1007/s11001-010-9107-8

Grindlay, N. R., Mann, P., Dolan, J. F., & van Gestel, J. P. (2005). Neotectonics and subsidence of the northern Puerto Rico-Virgin Islands margin in response to the oblique subduction of high-standing ridges. *Active Tectonics and Seismic Hazards of Puerto Rico, the Virgin Islands, and Offshore Areas*, *385*, 31–60.

Helsley, C. E. (1960). *Geology of the British Virgin Islands*. Princeton University.

Hu, H. Y., Stern, R. J., Rojas-Agramonte, Y., & Garcia-Casco, A. (2022). Review of geochronologic and geochemical data of the Greater Antilles volcanic arc and implications for the evolution of oceanic arcs. *Geochemistry, Geophysics, Geosystems*, *23*(4), e2021GC010148. https://doi.org/10.1029/2021GC010148

Iturralde-Vinent, M., & MacPhee, R. D. (1999). Paleogeography of the Caribbean region: Implications for Cenozoic biogeography. *Bulletin of the AMNH*, 238.

Iturralde-Vinent, M. A. (1994). Cuban geology: A new plate-tectonic synthesis. *Journal of Petroleum Geology*, *17*(1), 39–69. https://doi.org/10.1111/j.1747-5457.1994.tb00113.x

Iturralde-Vinent, M. A., Otero, C. D., García-Casco, A., & van Hinsbergen, D. J. (2008). Paleogene foredeep basin deposits of North-central Cuba: A record of arc-continent collision between the Caribbean and North American plates. *International Geology Review*, *50*(10), 863–884. https://doi.org/10.2747/0020-6814.50.10.863

Kerr, A. C., Tarney, J., Marriner, G. F., Nivia, A., & Saunders, A. D. (1997). The Caribbean-Colombian Cretaceous igneous province: The internal anatomy of an oceanic plateau. *Geophysical monograph-American Geophysical Union*, *100*, 123–144.

Kirschvink, J. (1980). The least-squares line and plane and the analysis of palaeomagnetic data. *Geophysical Journal International*, *62*(3), 699–718. https://doi.org/10.1111/j.1365-246x.1980.tb02601.x

Koymans, M. R., Langereis, C. G., Pastor-Galán, D., & van Hinsbergen, D. J. (2016). Paleomagnetism.org: An online multi-platform open source environment for paleomagnetic data analysis [Software], *93*, 127–137. https://doi.org/10.1016/j.cageo.2016.05.007

Koymans, M. R., van Hinsbergen, D. J. J., Pastor-Galán, D., Vaes, B., & Langereis, C. G. (2020). Towards FAIR paleomagnetic data management through Paleomagnetism.org 2.0. *Geochemistry, Geophysics, Geosystems*, *21*(2), e2019GC008838. https://doi.org/10.1029/2019GC008838

Laó-Dávila, D. A. (2014). Collisional zones in Puerto Rico and the northern Caribbean. *Journal of South American Earth Sciences*, *54*, 1–19. https://doi.org/10.1016/j.jsames.2014.04.009

Laurencin, M., Marcaillou, B., Graindorge, D., Klingelhoefer, F., Lallemand, S., Laigle, M., & Lebrun, J. F. (2017). The polyphased tectonic evolution of the Anegada Passage in the northern Lesser Antilles subduction zone. *Tectonics*, *36*(5), 945–961. https://doi.org/10.1002/2017tc004511

Laurencin, M., Marcaillou, B., Graindorge, D., Lebrun, J. F., Klingelhoefer, F., Boucard, M., et al. (2019). The bunce fault and strain partitioning in the northern Lesser Antilles. *Geophysical Research Letters*, *46*(16), 9573–9582. https://doi.org/10.1029/2019GL083490

Legendre, L., Philippon, M., Münch, P., Leticee, J. L., Noury, M., Maincent, G., et al. (2018). Trench bending initiation: Upper plate strain pattern and volcanism. Insights from the Lesser Antilles arc, St. Barthelemy island, French West Indies. *Tectonics*, *37*(9), 2777–2797. https://doi.org/10.1029/2017TC004921

Leroy, S., de Lépinay, B. M., Mauffret, A., & Pubellier, M. (1996). Structural and tectonic evolution of the eastern Cayman Trough (Caribbean Sea) from seismic reflection data. *AAPG Bulletin*, *80*(2), 222–247.

Leroy, S., Ellouz-Zimmermann, N., Corbeau, J., Rolandone, F., de Lepinay, B. M., Meyer, B., et al. (2015). Segmentation and kinematics of the North America-Caribbean plate boundary offshore Hispaniola. *Terra Nova*, *27*(6), 467–478. https://doi.org/10.1111/ter.12181

Leroy, S., Mauffret, A., Patriat, P., & Mercier de Lépinay, B. (2000). An alternative interpretation of the Cayman trough evolution from a reidentification of magnetic anomalies. *Geophysical Journal International*, *141*(3), 539–557. https://doi.org/10.1046/j.1365-246x.2000.00059.x

Lidiak, E. G., & Anderson, T. H. (2015). Evolution of the Caribbean plate and origin of the Gulf of Mexico in light of plate motions accommodated by strike-slip faulting. https://doi.org/10.1130/2015.2513(01)

López, A. M., Stein, S., Dixon, T., Sella, G., Calais, E., Jansma, P., et al. (2006). Is there a northern Lesser Antilles forearc block? *Geophysical Research Letters*, *33*(7), L07313. https://doi.org/10.1029/2005gl025293

Macdonald, R., Hawkesworth, C. J., & Heath, E. (2000). The Lesser Antilles volcanic chain: A study in arc magmatism. *Earth-Science Reviews*, *49*(1–4), 1–76. https://doi.org/10.1016/s0012-8252(99)00069-0

MacDonald, W. D. (1980). Net tectonic rotation, apparent tectonic rotation, and the structural tilt correction in paleomagnetic studies. *Journal of Geophysical Research*, *85*(B7), 3659–3669. https://doi.org/10.1029/jb085ib07p03659

Mann, P. (2007). Overview of the tectonic history of northern Central America. https://doi.org/10.1130/2007.2428(01)

Mann, P., & Burke, K. (1984). Neotectonics of the Caribbean. *Reviews of Geophysics*, *22*(4), 309–362. https://doi.org/10.1029/rg022i004p00309

Mann, P., Calais, E., Ruegg, J. C., DeMets, C., Jansma, P. E., & Mattioli, G. S. (2002). Oblique collision in the northeastern Caribbean from GPS measurements and geological observations. *Tectonics*, *21*(6), 7–1. https://doi.org/10.1029/2001TC001304

Mann, P., Hippolyte, J. C., Grindlay, N. R., & Abrams, L. J. (2005). Neotectonics of southern Puerto Rico and its offshore margin. https://doi.org/10.1130/0-8137-2385-X.173

Mauffret, A., & Leroy, S. (1997). Seismic stratigraphy and structure of the Caribbean igneous province. *Tectonophysics*, *283*(1–4), 61–104. https://doi.org/10.1016/s0040-1951(97)00103-0

Mauffret, A., & Leroy, S. (1999). Neogene intraplate deformation of the Caribbean plate at the Beata Ridge. In *Sedimentary basins of the world* (Vol. 4, pp. 627–669). Elsevier.

McFadden, P. L., & McElhinny, M. W. (1988). The combined analysis of remagnetization circles and direct observations in palaeomagnetism. *Earth and Planetary Science Letters*, *87*(1–2), 161–172. https://doi.org/10.1016/0012-821x(88)90072-6

Mondziel, S., Grindlay, N., Mann, P., Escalona, A., & Abrams, L. (2010). Morphology, structure, and tectonic evolution of the Mona canyon (northern Mona Passage) from multibeam bathymetry, side-scan sonar, and seismic reflection profiles. *Tectonics*, *29*(2). https://doi.org/10.1029/2008TC002441

Montes, C., Rodriguez-Corcho, A. F., Bayona, G., Hoyos, N., Zapata, S., & Cardona, A. (2019). Continental margin response to multiple arc-continent collisions: The northern Andes-Caribbean margin. *Earth-Science Reviews*, *198*, 102903. https://doi.org/10.1016/j.earscirev.2019.102903

Montheil, L. (2023). NE Caribbean paleomagnetic dataset [Dataset]. Zenodo. https://doi.org/10.5281/zenodo.7791447

Montheil, L., Philippon, M., Cornée, J. J., BouDagher-Fadel, M., van Hinsbergen, D. J., Camps, P., et al. (2023). Geological architecture and history of the Antigua volcano and carbonate platform: Was there an Oligo– Miocene lull in Lesser Antilles arc magmatism? *GSA Bulletin*. https://doi.org/10.1130/B36465.1

Mullender, T. A., Frederichs, T., Hilgenfeldt, C., de Groot, L. V., Fabian, K., & Dekkers, M. J. (2016). Automated paleomagnetic and rock magnetic data acquisition with an in-line horizontal "2 G" system. *Geochemistry, Geophysics, Geosystems*, *17*(9), 3546–3559. https://doi.org/10.1002/2016GC006436

Nagle, F., Stipp, J. J., & Fisher, D. E. (1976). K-Ar geochronology of the Limestone Caribbees and Martinique, Lesser Antilles, West Indies. *Earth and Planetary Science Letters*, *29*(2), 401–412. https://doi.org/10.1016/0012-821x(76)90145-x

Noury, M., Philippon, M., Cornée, J. J., Bernet, M., Bruguier, O., Montheil, L., et al. (2021). Evolution of a shallow volcanic arc pluton during Arc migration: A tectono-thermal integrated study of the St. Martin granodiorites (northern lesser Antilles). *Geochemistry, Geophysics, Geosystems*, *22*(12), e2020GC009627. https://doi.org/10.1029/2020GC009627

Ogg, J. G. (2020). Geomagnetic polarity time scale. In *Geologic time scale 2020* (pp. 159–192). Elsevier. https://doi.org/10.1016/B978-0-12-824360-2.00005-X

Oliveira de Sá, A., d'Acremont, E., Leroy, S., & Lafuerza, S. (2021). Polyphase deformation and strain migration on the septentrional-Oriente Fault Zone in the windward passage, northern Caribbean Plate boundary. *Tectonics*, *40*(8), e2021TC006802. https://doi.org/10.1029/2021tc006802

Ortega-Ariza, D., Franseen, E. K., Santos-Mercado, H., Ramírez-Martínez, W. R., & Core-Suárez, E. E. (2015). Strontium isotope stratigraphy for Oligocene-Miocene carbonate systems in Puerto Rico and the Dominican Republic: Implications for Caribbean processes affecting depositional history. *The Journal of Geology*, *123*(6), 539–560. https://doi.org/10.1086/683335

Padron, C., Klingelhoefer, F., Marcaillou, B., Lebrun, J.-F., Lallemand, S., Garrocq, C., et al. (2021). Deep structure of the Grenada Basin from wide-angle seismic, bathymetric and gravity data. *Journal of Geophysical Research: Solid Earth*, *126*(2), e2020JB020472. https://doi.org/10.1029/2020JB020472

Philippon, M., Cornée, J. J., Münch, P., van Hinsbergen, D. J., Boudagher-Fadel, M., Gailler, L., et al. (2020). Eocene intra-plate shortening responsible for the rise of a faunal pathway in the northeastern Caribbean realm. *PLoS One*, *15*(10), e0241000. https://doi.org/10.1371/journal.pone.0249163

Philippon, M., & Corti, G. (2016). Obliquity along plate boundaries. *Tectonophysics*, *693*, 171–182. https://doi.org/10.1016/j.tecto.2016.05.033

Philippon, M., van Hinsbergen, D. J., Boschman, L. M., Gossink, L. A., Cornée, J. J., BouDagher-Fadel, M., et al. (2020). Caribbean intra-plate deformation: Paleomagnetic evidence from St. Barthélemy island for Post-Oligocene rotation in the Lesser Antilles forearc. *Tectonophysics*, *777*, 228323. https://doi.org/10.1016/j.tecto.2020.228323

Pindell, J., & Dewey, J. F. (1982). Permo-Triassic reconstruction of Western Pangea and the evolution of the Gulf of Mexico/Caribbean region. *Tectonics*, *1*(2), 179–211. https://doi.org/10.1029/tc001i002p00179

Pindell, J. L., & Kennan, L. (2009). Tectonic evolution of the Gulf of Mexico, Caribbean and northern south America in the mantle reference frame: An update. *Geological Society, London, Special Publications*, *328*(1), 1–55. https://doi.org/10.1144/SP328.1

Rankin, D. W. (2002). Geology of St. John, US Virgin Islands.

Reid, J. A., Plumley, P. W., & Schellekens, J. H. (1991). Paleomagnetic evidence for late Miocene counterclockwise rotation of north coast carbonate sequence, Puerto Rico. *Geophysical Research Letters*, *18*(3), 565–568. https://doi.org/10.1029/91GL00401

Renken, R. A., Ward, W. C., Gill, I. P., Gómez-Gómez, F., & Rodríguez-Martínez, J. (2002). Geology and hydrogeology of the Caribbean islands aquifer system of the commonwealth of Puerto Rico and the US Virgin Islands.

Rodríguez-Zurrunero, A., Granja-Bruña, J. L., Carbó-Gorosabel, A., Muñoz-Martín, A., Gorosabel-Araus, J. M., de la Peña, L. G., et al. (2019). Submarine morpho-structure and active processes along the North American-Caribbean plate boundary (Dominican Republic sector). *Marine Geology*, *407*, 121–147. https://doi.org/10.1016/j.margeo.2018.10.010

Román, Y. A., Pujols, E. J., Cavosie, A. J., & Stockli, D. F. (2021). Timing and magnitude of progressive exhumation and deformation associated with Eocene arc-continent collision in the NE Caribbean plate. *GSA Bulletin*, *133*(5–6), 1256–1266. https://doi.org/10.1130/B35715.1

Romito, S., & Mann, P. (2021). Tectonic terranes underlying the present-day Caribbean plate: Their tectonic origin, sedimentary thickness, subsidence histories and regional controls on hydrocarbon resources. *Geological Society, London, Special Publications*, *504*(1), 343–377. https://doi.org/10.1144/sp504-2019-221

Rowley, D. B. (2019). Comparing paleomagnetic study means with apparent wander paths: A case study and paleomagnetic test of the Greater India versus Greater Indian Basin hypotheses. *Tectonics*, *38*(2), 722–740. https://doi.org/10.1029/2017TC004802

Schrecengost, K. L., Glazner, A. F., & Coleman, D. S. (2009). Geochemistry and geochronology of the Virgin Islands Batholith. In *AGU fall Meeting Abstracts* (pp. T53A–T1555).

Schwindrofska, A., Hoernle, K., van den Bogaard, P., Hauff, F., & Werner, R. (2016). Submarine structures of the Caribbean Large Igneous Province: Age and geochemistry of the Beata Ridge and Hess Escarpment.

Smith, A. L., Schellekens, J. H., & Díaz, A. L. M. (1998). Batholiths as markers of tectonic change. *Tectonics and geochemistry of the northeastern Caribbean*, *322*, 99.

Speed, R. C., Burmester, R. F., & Beck, M. E., Jr. (1997). Paleomagnetism of Eocene basalts of Mayreau, West Indies: Implications for contrasts in tectonic rotation in the southeastern Caribbean. *International Geology Review*, *39*(1), 82–95. https://doi.org/10.1080/00206819709465260

Steel, I., & Davison, I. (2021). Map of the geology of the Northern Caribbean and the Greater Antillean Arc.

Symithe, S., Calais, E., De Chabalier, J. B., Robertson, R., & Higgins, M. (2015). Current block motions and strain accumulation on active faults in the Caribbean. *Journal of Geophysical Research: Solid Earth*, *120*(5), 3748–3774. https://doi.org/10.1002/2014JB011779

Tauxe, L., & Kent, D. V. (2004). A simplified statistical model for the geomagnetic field and the detection of shallow bias in paleomagnetic inclinations: Was the ancient magnetic field dipolar? https://doi.org/10.7916/D81N89JT

ten Brink, U., Wei, Y., Fan, W., Granja-Bruña, J. L., & Miller, N. (2020). Mysterious tsunami in the Caribbean Sea following the 2010 Haiti earthquake possibly generated by dynamically triggered early aftershocks. *Earth and Planetary Science Letters*, *540*, 116269.

ten Brink, U. S., Marshak, S., & Bruña, J. L. G. (2009). Bivergent thrust wedges surrounding oceanic island arcs: Insight from observations and sandbox models of the northeastern Caribbean plate. *Geological Society of America Bulletin*, *121*(12), 1522–1536. https://doi.org/10.1130/b26512.1

Torsvik, T. H., Van Der Voo, R., Preeden, U., Mac Niocaill, C., Steinberger, B., Doubrovine, P. V., et al. (2012). Phanerozoic polar wander, palaeogeography and dynamics. *Earth-Science Reviews*, *114*(3–4), 325–368. https://doi.org/10.1016/j.earscirev.2012.06.007

Vaes, B., Gallo, L. C., & van Hinsbergen, D. J. (2022). On pole position: Causes of dispersion of the paleomagnetic poles behind apparent polar wander paths. *Journal of Geophysical Research: Solid Earth*, *127*(4), e2022JB023953. https://doi.org/10.1029/2022JB023953

Vaes, B., Li, S., Langereis, C. G., & van Hinsbergen, D. J. (2021). Reliability of palaeomagnetic poles from sedimentary rocks. *Geophysical Journal International*, *225*(2), 1281–1303. https://doi.org/10.1093/gji/ggab016

van Benthem, S., Govers, R., Spakman, W., & Wortel, R. (2013). Tectonic evolution and mantle structure of the Caribbean. *Journal of Geophysical Research: Solid Earth*, *118*(6), 3019–3036. https://doi.org/10.1002/jgrb.50235

van Fossen, M. C., Channell, J. E., & Schellekens, J. H. (1989). Paleomagnetic evidence for Tertiary anticlockwise rotation in southwest Puerto Rico. *Geophysical Research Letters*, *16*(8), 819–822. https://doi.org/10.1029/GL016i008p00819

van Gestel, J. P., Mann, P., Dolan, J. F., & Grindlay, N. R. (1998). Structure and tectonics of the upper Cenozoic Puerto Rico-Virgin Islands carbonate platform as determined from seismic reflection studies. *Journal of Geophysical Research*, *103*(B12), 30505–30530. https://doi.org/10.1029/98jb02341

van Hinsbergen, D. J., De Groot, L. V., van Schaik, S. J., Spakman, W., Bijl, P. K., Sluijs, A., et al. (2015). A paleolatitude calculator for paleoclimate studies. *PLoS One*, *10*(6), e0126946. https://doi.org/10.1371/journal.pone.0126946

van Rijsingen, E. M., Calais, E., Jolivet, R., de Chabalier, J. B., Jara, J., Symithe, S., et al. (2021). Inferring interseismic coupling along the Lesser Antilles arc: A Bayesian approach. *Journal of Geophysical Research: Solid Earth*, *126*(2), e2020JB020677. https://doi.org/10.1029/2020JB020677

Wallace, L. M., Ellis, S., & Mann, P. (2009). Collisional model for rapid fore-arc block rotations, arc curvature, and episodic back-arc rifting in subduction settings. *Geochemistry, Geophysics, Geosystems*, *10*(5). https://doi.org/10.1029/2008gc002220

Ward, W. C., Scharlach, R. A., Hartley, J. R., Renken, R. A., Black, B. A., Gill, I. P., et al. (2002). Geology of the north coast ground-water province of Puerto Rico. In R. A. Renken, W. C. Ward, I. P. Gill, F. Gomez-Gomez, & J. Rodriguez-Martinez (Eds.), *Geology and hydrogeology of the Caribbean Islands aquifer system of the Commonwealth of Puerto Rico and the US Virgin Islands* (pp. 45–76).

Wessels, R. J. (2019). Strike-slip fault systems along the northern Caribbean plate boundary. In *Transform Plate boundaries and fracture zones* (pp. 375–395). Elsevier.

Wilson, F. H., Orris, G., & Gray, F. (2019). *Preliminary geologic map of the Greater Antilles and the Virgin Islands*. US Geological Survey Open-File Report.1036.

Zijderveld, J. D. A. (1967). AC demagnetization of rocks: Analysis of results. In *Methods in paleomagnetism DW Collinson, KM Creer* (pp. 254–286). SK Runcorn.